Mesozoic extensional brittle tectonics of the Arabian passive margin, inverted in the Zagros collision (Iran, interior Fars)

PAYMAN NAVABPOUR[1]*, JACQUES ANGELIER[2†] & ERIC BARRIER[3]

[1]*Universität Jena, Institut für Geowissenschaften, Burgweg 11, D-07749 Jena, Germany*

[2]*Géoscience Azur, La Darse, BP 48, 06235 Villefranche-Sur-Mer Cedex, France*

[3]*Université Pierre et Marie Curie, Case 129, 75252 Paris Cedex 05, France*

**Corresponding author (e-mail: payman.navabpour@gmail.com)*

†Deceased

Abstract: The present Zagros mountain belt of SW Iran is known to be the former NE Arabian passive continental margin of the southern Neo-Tethyan basin, which originated by Permian–Triassic rifting, and has a late Cenozoic collisional imbricate structure. We carried out brittle tectonic analyses of syndepositional normal fault slip data in the High Zagros Belt of the Fars Province to reconstruct the extensional deformation of the passive margin during the Mesozoic era in terms of stress tensor inversion. This reconstruction revealed two main directions of extension, developing from a north–south margin-oblique trend to a NE–SW margin-perpendicular one. Considering the basement structures and the existence of the basal Infracambrian salt detachment, we infer that a transtensional extension could have initiated two major periods of crustal stretching: a Permian–Triassic thick-skinned phase with the basement faults developing in an oblique rifting, and a Mesozoic thin-skinned phase with the sedimentary cover being affected by successive extensional structures and block tilting. This extensional tectonic history probably continued during the early Tertiary period, prior to the continental collision. Fault slip geometries and structural patterns of both the Mesozoic extension and the late Cenozoic compression indicate inversion of the inherited structures in the Zagros collision during the subsequent thin- and thick-skinned stages of crustal shortening.

The Zagros fold-and-thrust belt of Iran is a result of the Alpine orogenic events (Ricou *et al*. 1977) in the Alpine–Himalayan mountain range. It extends in a NW–SE direction from eastern Turkey to the Strait of Hormuz in southern Iran (Fig. 1). The High Zagros Belt (HZB, also known as the Imbricate Zone) marks the northeastern part of the former Arabian passive margin, which is separated from the Iranian plate along the Main Zagros Thrust (MZT) and the Main Recent Fault (MRF; Braud 1971; Tchalenko & Braud 1974; Berberian 1995). The two major parallel domains of the Sanandaj–Sirjan Metamorphic Zone (SSMZ) and the Urumieh–Dokhtar Magmatic Arc (UDMA), to the NE of the MZT, are presumed to be the result of NE-dipping subduction of the Neo-Tethyan oceanic crust beneath the Iranian continental active margin (Berberian & King 1981). The subduction process started in the late Jurassic period (Stampfli & Borel 2002) and terminated with the continental collision between the Arabian and Iranian plates in Oligocene–Miocene times (Sherkati & Letouzey 2004; Agard *et al*. 2005).

SW of the HZB, the belt is characterized by the major morphotectonic units of the Zagros Simply Fold Belt (ZSFB), Dezful Embayment and the Persian Gulf–Mesopotamian Lowland. The High Zagros Fault (HZF) marks the ZSFB–HZB boundary, with a concentration of seismic activity mainly to the SW (Talebian & Jackson 2004). From NW to SE, the ZSFB itself is divided into major sub-areas of the Lurestan Area, Izeh Zone and the Fars Arc, by the transverse strike-slip faults of the Balarud, Izeh and Kazerun Fault Zones, respectively. The Mountain Front Fault (MFF) bounds the ZSFB to the SW and separates it from the Dezful Embayment. The Zagros Front separates the Persian Gulf–Mesopotamian basin from the entire mountain belt. The presence of all these major belt-parallel and belt-oblique fault zones (Fig. 1), that are known to be pre-existing deep-seated crustal structures, facilitated different morphotectonic developments of the belt segments and highlighted significant differences in earlier palaeostratigraphic history and structural style (Berberian 1995; Sepehr & Cosgrove 2004).

Although the tectonostratigraphic evolution and deformation styles of the Zagros mountain belt have been studied in detail from stratigraphical, structural, seismic and geophysical points of view,

From: LETURMY, P. & ROBIN, C. (eds) ***Tectonic and Stratigraphic Evolution of Zagros and Makran during the Mesozoic–Cenozoic***. Geological Society, London, Special Publications, 330, 65–96.
DOI: 10.1144/SP330.5 0305-8719/10/$15.00

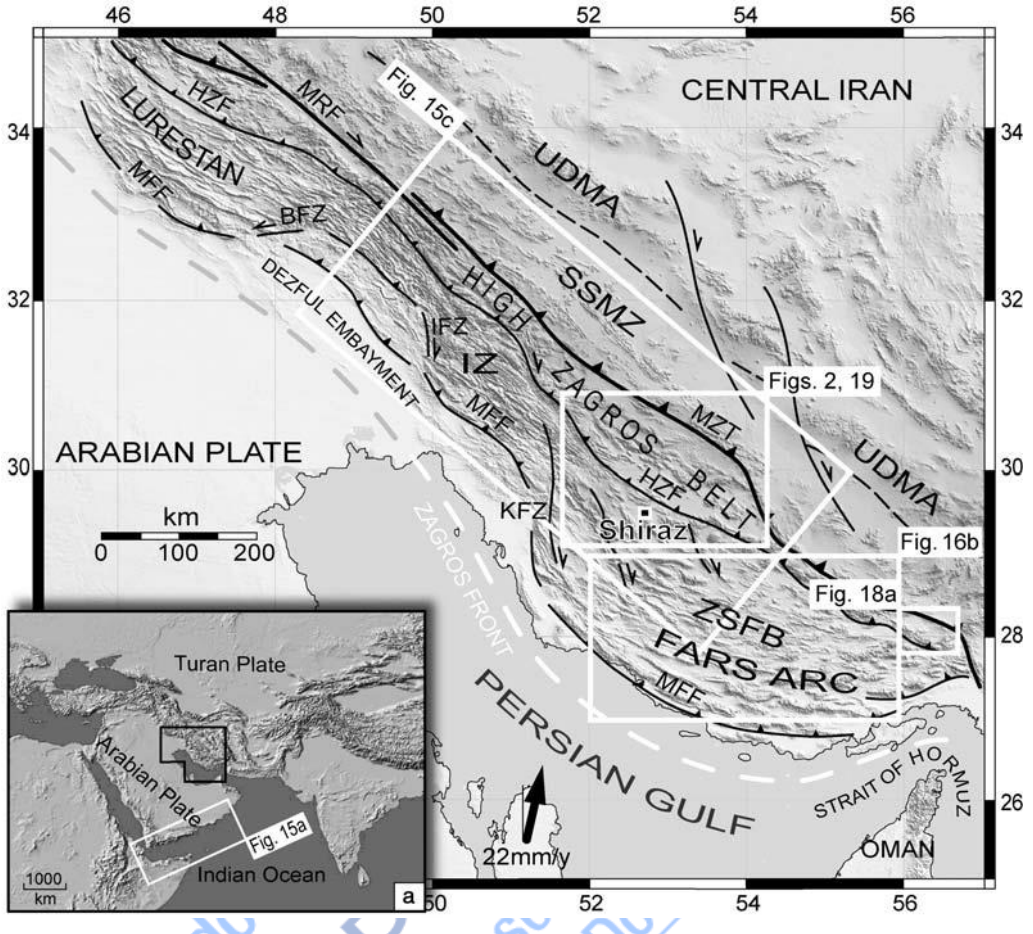

Fig. 1. Index map of the study area within the Zagros fold-and-thrust belt (from Navabpour *et al.* 2007*a*), showing the structural domains in SW Iran. Topography is from GTOPO30. UDMA, Urumieh – Dokhtar Magmatic Arc; SSMZ, Sanandaj – Sirjan Metamorphic Zone; MZT, Main Zagros Thrust; MRF, Main Recent Fault; HZF, High Zagros Fault; ZSFB, Zagros Simply Folded Belt; MFF, Mountain Front Fault; IZ, Izeh Zone; BFZ, Balarud Fault Zone; IFZ, Izeh Fault Zone; KFZ, Kazerun Fault Zone. Black arrow indicates GPS convergence vector from Vernant *et al.* (2004). Inset (a) is regional location map.

almost no attempt has been made to analyse the evolution of the HZB during the tectonic history of the NE Arabian Passive Margin (NEAPM) in terms of brittle tectonics. In this paper, we aim at deciphering the Mesozoic extensional brittle tectonics of the HZB of interior Fars (Fig. 1). Our study is primarily based on systematic stress inversion of brittle tectonic data with particular attention to the Mesozoic syndepositional faulting that reflects deep-seated extensional structures during the history of the NEAPM. However, the extensional history of the HZB is not limited to the Mesozoic era. We also observed Cenozoic normal faults associated with tension cracks that mainly developed as a function of the Cenozoic compressional deformation in this region (see Navabpour *et al.* 2007*a*).

Geological setting

The HZB is the most uplifted and eroded part of the Zagros mountain belt. Folds and thrusts trending NW – SE are the most common tectonic features of the HZB in the study area (Fig. 2). These features change into a highly imbricate structure to the NE (Molinaro *et al.* 2004, 2005*a*). Most of the affected rock units are shelf and open marine limestones and marls of the Mesozoic Arabian passive margin. Towards the SW, in the ZSFB, large folds have

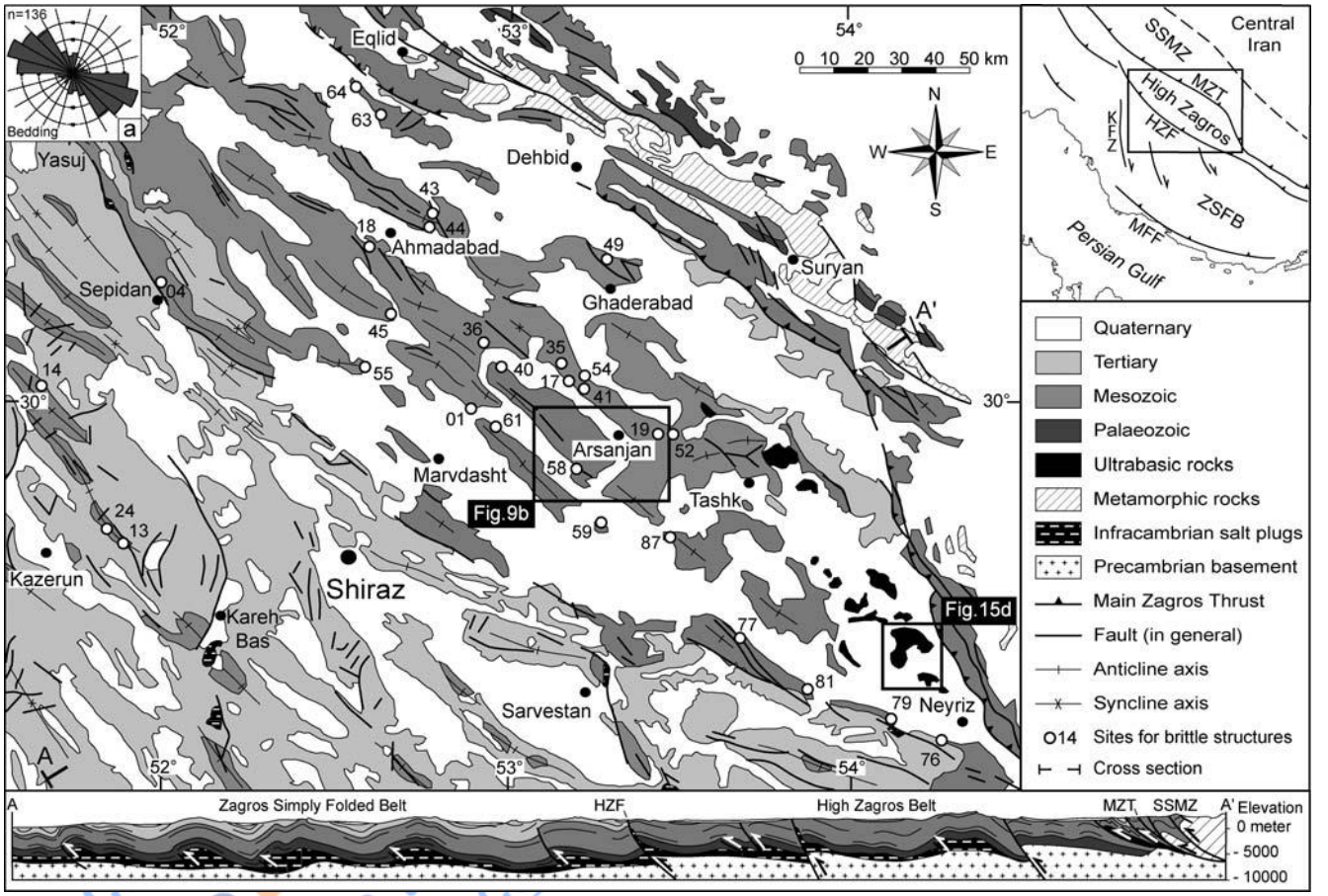

Fig. 2. Geological map of the study area in the interior Fars (from Navabpour *et al*. 2007*a*), showing the position of the sites where brittle structures were collected and measured. The map is mainly redrawn and simplified based on the geological map of NIOC (1977) with some changes based on NIOC (1979) and GSI (1985, 1990). The map is based on the major difference in lithology from the Palaeozoic and metamorphic rocks of the SSMZ to the Mesozoic rocks of the HZB and the Tertiary rocks of the ZSFB. AA′, location of cross-section in the map. Inset (a) shows the strike rose distribution of the folded strata (*n* ¼ 136) with an average trend of N123**8**. Stratigraphic details are given in Figure 3. Location is shown in Figure 1; abbreviations are as in Figure 1.

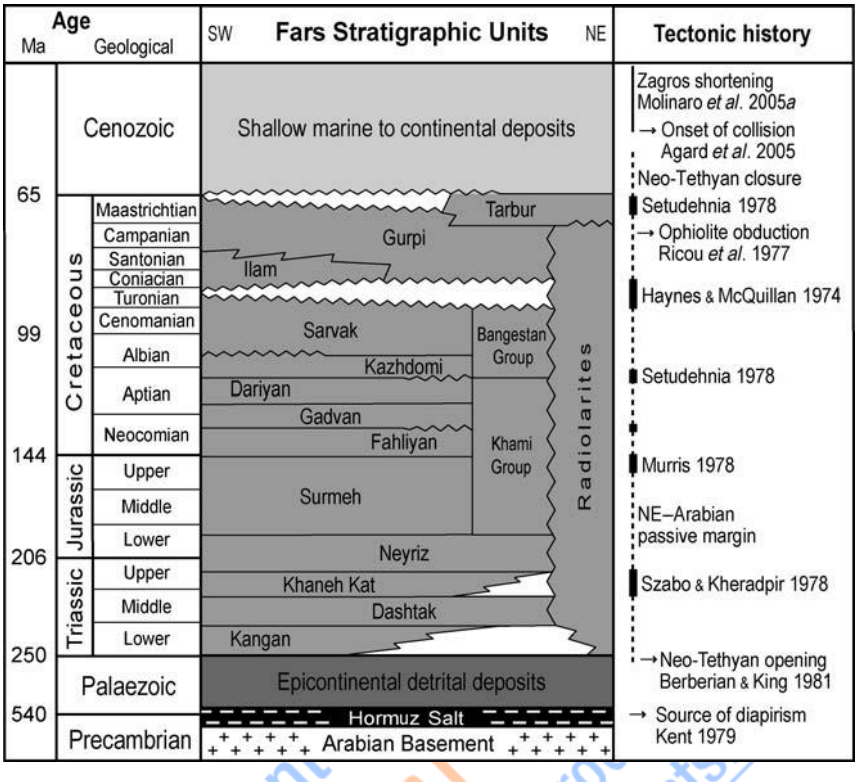

Fig. 3. Stratigraphic chart of the Fars region modified and simplified from Beydoun *et al.* (1992) and Motiei (1993). Absolute ages are from Palmer & Geissman (1999). Summary of tectonic history is added for a more complete account. Bold black lines show the various reported unconformities during the time of existence of the NEAPM (dashed line).

affected the shallow water carbonates and the clastic deposits of the Tertiary period, which belong to the platform domain of the Arabian margin. These two major domains are separated by the HZF (Figs 1 & 2). In the study area, the metamorphic rocks of the SSMZ thrust over the HZB along the MZT, which is expected to be the surface trace of the Arabia – Eurasia suture zone (Berberian & King 1981; Paul *et al.* 2003, 2006; Agard *et al.* 2005, 2006). In addition, a narrow belt of ophiolite and radiolarite nappe is situated between the MZT and the HZB to the east of the area (Fig. 2). This thrust sheet of ophiolite and radiolarite is considered as a remnant of the Neo-Tethyan oceanic crust (Ricou 1968).

Stratigraphy

The entire Zagros belt is formed by more than 10 km thickness of Palaeozoic – Cenozoic sedimentary layers, detached from metamorphic continental basement above the thick Infracambrian Hormuz Salt Formation (Falcon 1974) (Figs 2 & 3). Geological evidence suggests that Iran was a part of the Afro-Arabian continental platform, at least from the late Precambrian to late Palaeozoic times, with epicontinental detrital deposits (Stocklin 1968; Nabavi 1976). During the Permian period, the Arabian foreland (i.e. the HZB) gradually subsided and the sea invaded most of the area. This event is marked by a significant change in sedimentation over the Arabian foreland, from dominantly Palaeozoic clastic sediments to the carbonate series of Permian, Mesozoic and Tertiary times (Powers 1968; see also Fig. 3). There is evidence of volcanic activity associated with the Permian – Triassic rifting in the HZB, where a few amygdaloidal basaltic flows of Permian age crop out (Thiele *et al.* 1968; Berberian 1977). In the NE of the HZB, the late Triassic black marls of the Arabian foreland are covered by a thick sequence of Jurassic – Cretaceous deep-sea red radiolarian chert and siliceous limestone (Ricou 1974, 1976) that belongs to the Neo-Tethyan oceanic environment (Berberian & King 1981; Ricou 1994).

To the SW, the Arabian foreland (i.e. the Zagros basin) steadily subsided along inherited faults during the Mesozoic era. The marine carbonate sedimentary regime persisted during the early Triassic period, with deposition of the Kangan Formation (Szabo & Kheradpir 1978; see also Fig. 3).

Regressive conditions then occurred in the middle Triassic period, resulting in deposition of the evaporites of the Dashtak Formation (Berberian & King 1981). In the HZB, an unconformity is present between the middle Triassic and Jurassic beds. Above the unconformity, the Liassic terrige- nous clastic deposits and the transitional terrigenous to open marine sediments of the Neyriz Formation accumulated (Szabo 1977; Szabo & Kheradpir 1978). Overlying the Neyriz Formation, the marine limestones and marls of the Khami Group (Middle Jurassic – Aptian; Fig. 3) reveal a steadily subsiding basin and continuous sedimentation in the interior Fars, during middle Jurassic – early Cre- taceous times (James & Wynd 1965; Setudehnia 1978).

In the interior Fars, the siltstones and iron-stained glauconitic sandstones found in the upper parts of the Fahliyan and Dariyan Formations indicate periods of regression, emergence and erosion in the Neocomian and Late Aptian, respectively (James & Wynd 1965; Setudehnia 1978). The sedimentation continued with the shallow marine shales and carbonates of the Bangestan Group (Albian – Turonian; Fig. 3). The conglomerates, breccia, ferruginous materials and a weathered zone on top of the Sarvak Formation indicate tectonic activity in most of the interior Fars in the Late Turonian (Berberian & King 1981). East of Arsanjan, a transition occurs between the iron-stained Turonian carbonate platform and deep-sea radiolarian sediments towards the NE (Fig. 2). A submarine channel filled with turbiditic carbonate breccia cut through the radiolarite unit (Haynes & McQuillan 1974). The late Cretaceous sedimentation in most parts of the Zagros basin usually began with neritic carbonates of the Ilam Formation (Santonian – Early Campanian). This carbonate sedimentation was followed by deeper water conditions, with marls and shales of the Gurpi Formation (Campanian – Maastrichtian), which covered almost the entire Zagros basin. In the late Maastrichtian, a general regression created a major Cretaceous – Cenozoic unconformity throughout the Zagros (James & Wynd 1965; Setudehnia 1978).

The Cenozoic era was characterized by a regional change in sedimentary facies, from an open marine to a continental environment. During this era, the Palaeocene – Eocene neritic shales and marls of the Pabdeh Formation changed to the Eocene – Oligocene shallow water limestones of the Jahrom and Asmari Formations and were covered by the Miocene evaporites and red beds of the Gachsaran – Agha Jari Formations and the Pliocene – Pleistocene molasse-type Bakhtyari conglomerates. All these facies changes involved angular unconformities that are thought to be the result of folding and erosion that originated from the Tertiary Neo-Tethyan closure process and collision between the Arabian and Iranian continental plates (Berberian & King 1981; Hessami *et al.* 2001).

Structures and tectonic setting

Most of the linear facies boundaries trending NW – SE and the related different subsidence rates during the Mesozoic era were the result of normal faulting parallel to the NEAPM (Berberian & King 1981; Koop & Stoneley 1982). This is supported by the idea that the present-day seismicity of the Zagros mountain belt is a result of inverse reactivation on pre-existing NE-dipping normal faults during the Cenozoic continental collision between the Arabian and Iranian plates and the following plate convergence (Jackson 1980; Jackson & McKenzie 1984). It has also been shown that the conglomerates on top of the Sarvak Formation in SE Zagros resulted from normal faulting within the sedimentary basin (Stoneley 1990).

According to Chauvet *et al.* (2004), syndepositional normal faults are observed in the Permian carbonate platform of Oman, south of the Hormuz Strait. Conjugate normal faults with metre-scale offsets and block tilting associated with extensional structures in that region indicate a north – south direction of extension. Those researchers have shown that the tilted structures, which were sealed by an unconformity associated with dolomitization, reveal a middle Permian extensional phase in the Arabian margin during the first stage of the Neo-Tethyan rifting. The analysis of seismic profiles revealed that the growth of the Permian – Triassic strata was related to the hanging wall of a buried normal fault in the Dezful Embayment (Sepehr & Cosgrove 2004), evidencing a Permian – Triassic extension in the Zagros. This evidence suggested that at that time the ZSFB was the domain of a fault-controlled horst-and-graben structure with a greater subsidence rate as compared with the HZB (Sepehr & Cosgrove 2004).

The relatively stable oceanic environment of the NEAPM was affected by a southwestward obduction of the Neo-Tethyan ophiolite – radiolarite nappe (the Semail Ocean of Stampfli 2000) in the late Cretaceous period (Béchennec *et al.* 1990; Breton *et al.* 2004). In the Neyriz area, the shallow water reef limestones of the Upper Campanian – Maastrichtian Tarbur Formation covered the ophiolitic thrust stack unconformably (Ricou 1974). The obduction of the ophiolites was thus thought to have occurred during the Late Santonian – Early Campanian (Berberian & King 1981), as the deposition of the Tarbur limestones postdates the emplacement of the ophiolite – radiolarite nappe. However, Stoneley (1990) believed that the emplacement of the ophiolites in the HZB was due to a change in the position of oceanic spreading axis to the south, uplifting of the Arabian shelf margin and a

subsequent southwestward gravitational sliding of the oceanic deposits over the shelf. He thus inferred that the emplacement of the ophiolites in the HZB differs from the tectonic compressive obduction that occurred in Oman.

The present-day morphotectonic features of the Zagros mountain belt (Berberian 1995) are a consequence of the late Cenozoic Neo-Tethyan closure and continental collision under a north – south plate convergence (McQuarrie *et al.* 2003; Agard *et al.* 2005). The angular unconformities and facies changes within the Cenozoic sedimentary sequence show that the folding process, which was initiated in the HZB in late Oligocene – early Miocene times (Sherkati *et al.* 2005), was a result of separate tectonic episodes during which the deformation front propagated from NE to SW (Hessami *et al.* 2001). In NW Zagros, the north – south plate convergence is partitioned into a belt-parallel right-lateral slip along the MRF and a belt-perpendicular shortening across the ZSFB (Talebian & Jackson 2004; Authemayou *et al.* 2006). In SE Zagros, structural studies have indicated that the belt has undergone two distinct thin- and thick-skinned north – south crustal shortening episodes since the Miocene epoch (Molinaro *et al.* 2005*a*; Sherkati *et al.* 2005; Mouthereau *et al.* 2007). This idea is consistent with the recent seismicity of the basement reverse faults under an overall north – south compression (Talebian & Jackson 2004). Detailed brittle tectonic reconstructions have shown that the late Cenozoic deformation involve an anticlockwise reorientation of the compressive stress trend, from a pre-folding NE – SW direction to a post-folding north – south one, associated with a more distributed strike-slip reactivation of the earlier reverse faults across the HZB of interior Fars (Navabpour *et al.* 2007*a*).

Brittle tectonic analysis and main extensional events

Not only do the tectonic events affecting the HZB differ in nature (compression, extension, wrench faulting), but they also show contrasting stress fields in the interior Fars. We used systematic brittle tectonic analyses, especially in terms of stress tensor inversion, to decipher the various extensional tectonic episodes that have affected the NEAPM during the Mesozoic era. The common steps in these analyses involve data collection in the field, data separation, age recognition, computation of the stress fields and finally characterization and classification of the various events. For most of the brittle structures that we studied, we collected fault slip data (oblique-slip, normal, strike-slip and reverse). These data include the orientation of fault surfaces, slickenside lineation and sense of motion indicators where available. Tension cracks were also abundant, but there are few data on pressure-solution seams. The bedding attitudes of the sedimentary units were recorded at all sites to reconstruct the initial pre-folding attitudes of strata and related brittle structures where appropriate.

Palaeostress reconstructions

Our palaeostress determinations are based on systematic use of the direct inversion method (Angelier 1984, 1990, 2002). Where data distribution did not allow a reliable stress tensor determination, we used the right dihedra method (Angelier & Mechler 1977). A widespread difficulty in palaeostress determinations was related to the heterogeneity of the datasets in the study area, which is often a result of two or more successive tectonic events involving polyphase brittle deformation. In such cases, computing an average stress regime was meaningless, and data separation into more mechanically homogeneous subsets was compulsory. These subsets fit the different stress states and may reveal distinct tectonic events. Various criteria are used in this relation, including crosscutting relationships between different brittle structures and successive striae observed on fault surfaces that indicate fault reactivation under a new stress field. In addition, the sedimentary layers have been subjected to faulting during both the basin sedimentation of the passive margin and the folding process of the collision. It was thus indispensable to pay close attention to geometrical and relative relationships between folds, brittle structures and syndepositional evidence. Particular attention was paid to the stratigraphic ages of affected rocks and the unconformities revealed by geological mapping (NIOC 1977, 1979; GSI 1985, 1990, 1996*a*, *b*, 1999, 2000*a* – *d*, 2001*a*, *b*). Such information led to more accurate dating of syndepositional tectonic events. The succession of compressional and extensional stress fields during the late Cenozoic collisional history of the HZB has already been discussed elsewhere (Authemayou *et al.* 2006; Navabpour *et al.* 2006, 2007*a*, *b*). Below, we present only the relevant brittle tectonic data used to reconstruct the various extensional events within the sedimentary basin of this area.

In the reconstruction of palaeostress directions, consideration of possible block rotation is crucial. In the absence of palaeomagnetic data, horizontal block rotations around vertical axes could not be reconstructed. Geologically, there is no evidence of block rotation related to the mountain-building process, because the trends of the late Cenozoic folds remained consistent throughout the HZB in the study area, as suggested by the rose diagram of the folded strata (Fig. 2a). Both the MZT and the HZF are thought to have acted as reverse faults

with no strike-slip movement during the late Cenozoic shortening, after the onset of collision (Molinaro *et al.* 2005*a*) under a general NE–SW direction of compression (Navabpour *et al.* 2007*a*). The earthquake focal mechanisms along the HZF invariably show reverse faulting (see Talebian & Jackson 2004) on pre-existing high-angle faults (Yamini-Fard *et al.* 2006) and thus do not confirm a major active strike-slip movement that could have induced large block rotations across the HZB of interior Fars even under the present-day north–south oblique convergence. Moreover, the consistency of the stress directions obtained from each brittle tectonic event (Navabpour *et al.* 2007*a*) suggests that no significant block rotation has occurred since the Miocene compression, at least in the study region, where sites are densely distributed. However, further to the south, a possible horizontal rotation of the sedimentary cover is evidenced by magnetic fabric studies of the late Tertiary sandstones in the ZSFB of the Fars Arc (Bakhtari *et al.* 1998; Aubourg *et al.* 2004). We thus infer that no major horizontal rotation around vertical axis has occurred in the study area, except the well-documented rotation of Arabia as a whole, which is revealed by plate kinematic reconstructions (e.g. Dercourt *et al.* 2000; McQuarrie *et al.* 2003). On the other hand, all the orientations referred to hereafter are corrected by back-tilting the strata to their initial horizontal attitudes to reconstruct the Mesozoic extensional events that gave way to deep-seated vertical block rotation around horizontal axes and related syndepositional normal faulting.

A summary of palaeostress reconstructions is provided for a more complete account (Table 1), in which data for each stress regime are presented based on their geographical positions and the stratigraphic age of the affected rocks. The geological situation of each site is indicated in the geological map (Fig. 2). As mentioned above, the relative relationships of different normal faults and syndepositional evidence are crucial. For this reason, these data are presented separately in the Table 1. The bedding attitude of each site is given to allow reconstruction of the initial horizontal attitudes of the related brittle structure (BS) with respect to local tilted strata. Calculated stress fields are defined by the direction and plunge of the principal stress axes (s_1, s_2 and s_3), method of analysis (M), number of data (N), ratio of the stress magnitude differences (F) and the reduced misfit angle (a), which is acceptable for $a \leq 25°$. In addition, a quality estimator (Q) is attached to each determination, because local results of the stress calculations cannot be regarded as equal in value. This quality estimator provides a multivariable evaluation between different stress solutions that strictly depends on quantitative (such as the number of acceptable data and the average misfit level) and semi-quantitative and qualitative aspects (such as the confidence level and accuracy of fault slip measurements). The reader is referred to Angelier (1984, 1990, 2002) for further details on the inversion parameters.

Identification of the Mesozoic extensions

To reconstruct the Mesozoic extensional tectonic history of the NEAPM we used syndepositional evidence within each stratigraphic sequence during which the normal faults have been developed. Two typical main features of such evidence are the sedimentary wedges on the hanging wall of normal faults (Nottvedt *et al.* 1995) and the tilted blocks bounded by normal faults subjected to local erosion and sealed by younger sedimentary layers (Leeder & Gawthorpe 1987). In the first case, during the development of listric normal faults within a sedimentary basin, the hanging-wall block tilts towards the footwall of the fault so that an asymmetric trough is generated. Continuing deposition then fills this asymmetric trough, creating a syntectonic sedimentary wedge. We used the presence of such sedimentary wedges to detect syndepositional normal faults (e.g. site 43; Fig. 4a). In the second case, an extensional episode creates a bookshelf structure with multiple tilted blocks and normal faults that is subsequently covered and sealed by younger sedimentary layers. The time span between the older and younger sediments constrains the age of the extensional event (e.g. site 45; Fig. 4b).

A difficulty in determining the age of extension arises in the absence of syndepositional evidence. In such a case, a systematic back-tilting can be applied for tilted strata (e.g. site 15; Fig. 5a), revealing the pre-tilt attitude of corresponding stress axes. Ambiguities may, however, occur. For instance, it may be difficult to distinguish between pre-tilt normal faults (indicating an early extension) and post-tilt reverse faults (related to a late compression), where the layers have been tilted by folding to a subvertical attitude. A set of conjugate-like normal faults that developed in the sedimentary basin can be observed as conjugate reverse faults at the present-day attitude in the nearly vertical fold flanks. However, a comparison between sites with a variety of stratal dips across the fold structure usually solves the ambiguity (Fig. 5b). Back-tilting the strata will in this case yield a consistent pre-fold attitude for the relevant extension (Fig. 5c). Despite these possibilities, some uncertainties remain where strata are horizontal (unfolded). In such cases, it may be almost impossible to determine the age of the extension by direct observation (except for the maximum age indicated by dating of the affected sedimentary rock). Because of these limitations,

Table 1. *Summary of geological position of brittle structures and reconstructed extensional stress regimes*

Stress regime	Location	Coordinates		Stratigraphic age	Bedding Strike/dip	Site no.	BS	M	*N*	s_1		s_2		s_3		*F*	*a*	*Q*
		Long. (E)	Lat. (N)							Dir.	Plunge	Dir.	Plunge	Dir.	Plunge			
Mesozoic syndepositional extensional regimes (Fig. 7)	NE Marvdasht	52.89	29.99	Alb. – Cenom.	014/13W	01	N*	DI	19	282	60	125	28	030	10	0.49	15	A
	NW Arsanjan	53.19	30.10	Aptian	167/10W	17	N*	DI	8	026	65	120	02	211	25	0.45	20	B
	E Arsanjan	53.45	29.92	Alb. – Cenom.	137/05E	19	N	DI	8	010	66	122	09	216	22	0.34	19	B
	E Kazerun	51.90	29.65	Camp. – Maas	149/12W	24	N*	DI	5	264	85	031	03	122	04	0.47	9	A
	NW Arsanjan	53.15	30.09	Aptian	124/33S	35	N*	RD	8	284	76	101	15	191	01	0.48		A
	N Marvdasht	52.91	30.11	Aptian	100/24N	36	N*	DI	10	343	79	098	05	189	10	0.46	11	A
	NW Arsanjan	53.20	30.10	Aptian	138/31W	41	N*	RD	26	331	85	120	04	210	03	0.61		A
	NE Ahmadabad	52.79	30.46	M. – L. Jurassic	032/35E	43	N*	DI	10	151	63	033	13	297	23	0.44	12	A
	NE Ahmadabad	52.77	30.44	M. – L. Jurassic	168/17E	44	N*	DI	10	144	78	272	07	003	09	0.50	9	A
	S Ahmadabad	52.67	30.22	Cenomanian	087/07S	45	N	RD	20	187	72	293	05	024	17	0.48		A
	E Arsanjan	53.45	29.92	Cenomanian	Horizontal	52	N	RD	5	139	86	312	04	042	01	0.49		B
	NW Marvdasht	52.59	30.10	Cenomanian	136/16E	55	N*	DI	10	037	66	269	15	174	18	0.50	5	A
	S Arsanjan	53.26	29.67	Cenomanian	113/34S	59	N*	DI	13	227	73	099	10	006	13	0.47	15	A
	S Eghlid	52.59	30.75	E. Jurassic	092/26N	63	N*	DI	8	359	77	105	04	195	13	0.47	17	B
	S Neyriz	54.19	29.18	Jurassic	096/43S	76	N*	RD	6	295	59	101	31	194	06	0.61		B
	S Neyriz	54.19	29.18	Jurassic	096/43S	76	N*	RD	2	194	00	284	64	104	27	0.63		C
	NE Sarvestan	53.59	29.45	M. – L. Triassic	178/33W	77	N*	DI	4	330	74	101	11	193	12	0.47	12	A
	S Neyriz	54.11	29.18	Jurassic	104/85N	79	N*	DI	8	001	77	266	01	176	13	0.50	9	A
	SW Tashk	53.44	29.66	E. Cretaceous	127/17N	87	N*	DI	25	055	77	271	10	180	07	0.51	11	A
Back-tilted pre-Cenozoic folding extensional regimes (Fig. 8)	N Sepidan	51.97	30.30	Cretaceous	100/26N	04	N*	DI	5	344	66	094	09	187	23	0.48	22	B
	W DashteArjan	51.93	29.63	Camp. – Maas.	028/03E	13	N	DI	13	335	81	121	08	211	05	0.44	13	A
	N Kazerun	51.66	30.02	Camp. – Maas.	142/63E	14	N*	DI	40	227	70	135	01	045	20	0.51	10	A
	SW Ahmadabad	52.58	30.39	Cenomanian	117/20N	18	N*	DI	8	065	67	272	20	179	09	0.52	13	A
	NE Marvdasht	52.93	30.11	Cenomanian	102/73N	40	N*	RD	5	246	55	116	24	014	24	0.53	25	B
	N Ghaderabad	53.30	30.33	Aptian	123/20N	49	N*	DI	15	229	63	105	16	008	21	0.37	19	B
	NW Arsanjan	53.20	30.10	Aptian	150/20W	54	N*	RD	11	330	74	123	15	215	07	0.73		B
	SW Arsanjan	53.16	29.85	M. – L. Jurassic	123/12N	58	N*	DI	13	234	79	121	04	030	10	0.44	22	B
	NE Marvdasht	52.94	29.95	Albian	135/66N	61	N*	RD	4	204	66	311	07	044	23	0.51		B
	SW Eghlid	52.53	30.81	E. Jurassic	141/37E	64	N*	DI	9	090	67	291	22	198	08	0.52	20	B
	W Neyriz	53.89	29.25	Cenomanian	125/43N	81	N*	DI	9	097	84	300	06	210	02	0.52	11	A

BS, brittle structures: N, normal faults (where * indicates back-tilted strata). M, method of stress determination (RD, right dihedra; DI, direct inversion); *N*, number of fault slip data; *F*, ratio of stress magnitude differences [$F = (s_2 - s_3)/(s_1 - s_3)$]; *a*, average angle between observed slip and computed shear in degrees (acceptable for $a \leq 25$); *Q*, quality of stress calculation (A, high; B, moderate; C, low). Bedding attitudes and stress axes are given after magnetic north correction. Site location is shown in Figure 2.

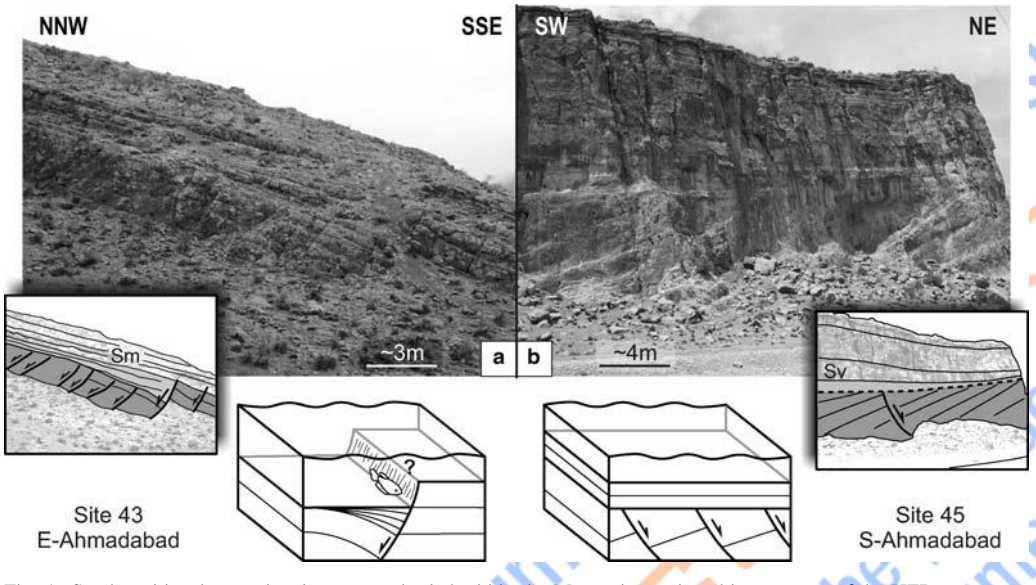

Fig. 4. Syndepositional extensional structures buried within the Mesozoic stratigraphic sequence of the HZB. (a) Sedimentary wedge in the hanging wall of a palaeo-submarine normal fault observed at site 43, revealing active extension during deposition of the Surmeh Formation (Sm) in the middle – late Jurassic period. (b) Tilted blocks along a normal fault within the Sarvak Formation (Sv) sealed by younger sedimentary layers of the same formation at site 45, indicating an intraformational angular unconformity (dashed line) during a middle Cretaceous phase of extension. In the insets, faulted key-beds are shown in dark grey whereas sedimentary wedges and unaffected beds are shown in light grey. Small 3D schemes of deformation are added for more detail. It should be noted that in each photograph the entire outcrop is formed of the same rock unit.

we paid special attention to syndepositional deformations that could be observed in the field.

For a complete account, we have provided some of the field examples of the Mesozoic syndepositional extensional structures, together with the stress tensors analysed after back-tilting the corresponding fault slip data (Fig. 6). For instance, at site 01, the upper layers of the Sarvak Formation show different thicknesses involved with normal faulting (Fig. 6a). This situation indicates that faulting was active during the Cenomanian. The stress tensor inversion of the normal faults at this site reveals a NE – SW direction for the extensional s_3 stress axis. At sites 17, 19 and 59, the faulted key-beds of the Sarvak and Dariyan Formations are sealed with unaffected upper layers of the same formations (Fig. 6b – d), indicating extensional tectonic activity during the deposition of these formations during the Cenomanian and Aptian, respectively. The stress tensor inversion of the corresponding normal faults reveals two NE – SW and north – south directions of extension. At sites 36 and 55, a sedimentary wedge is observed above the major normal faults within the Sarvak Formation (Fig. 6e, f), characterizing a north – south direction of extension. At site 77, the Jurassic limestones of the Surmeh Formation seal tilted blocks of the Upper Triassic Khaneh Kat Formation (Fig. 6g), indicating a north – south direction of extension. A syndepositional north – south direction of extension is also evidenced by normal faults within the Jurassic radiolarite layers of the Neo-Tethyan basin at site 79. The sedimentary layers at this site are folded and tilted to a subvertical present-day attitude (Fig. 6h), presenting conjugate reverse faults. However, after back-tilting the strata to a pre-fold horizontal situation, the unaffected uppermost layers agree with a syndepositional normal faulting.

Numerous outcrops throughout the study area revealed syndepositional Mesozoic normal faulting. Azimuthal distribution of the calculated stress axes for the corresponding fault slip data reveals two major north – south and NE – SW trends for the extensional s_3 stress axes after back-tilting correction (Fig. 7). The average trends of extension are N006E and N034E, respectively. These directions were reconstructed based on consideration of 85% of the Mesozoic syndepositional structures that could be identified as normal faults striking east – west and NW – SE, respectively. We also measured consistent brittle structures at some sites where no evidence of syntectonic sedimentation could be identified. Azimuthal distribution of calculated stress axes for the corresponding back-tilted fault

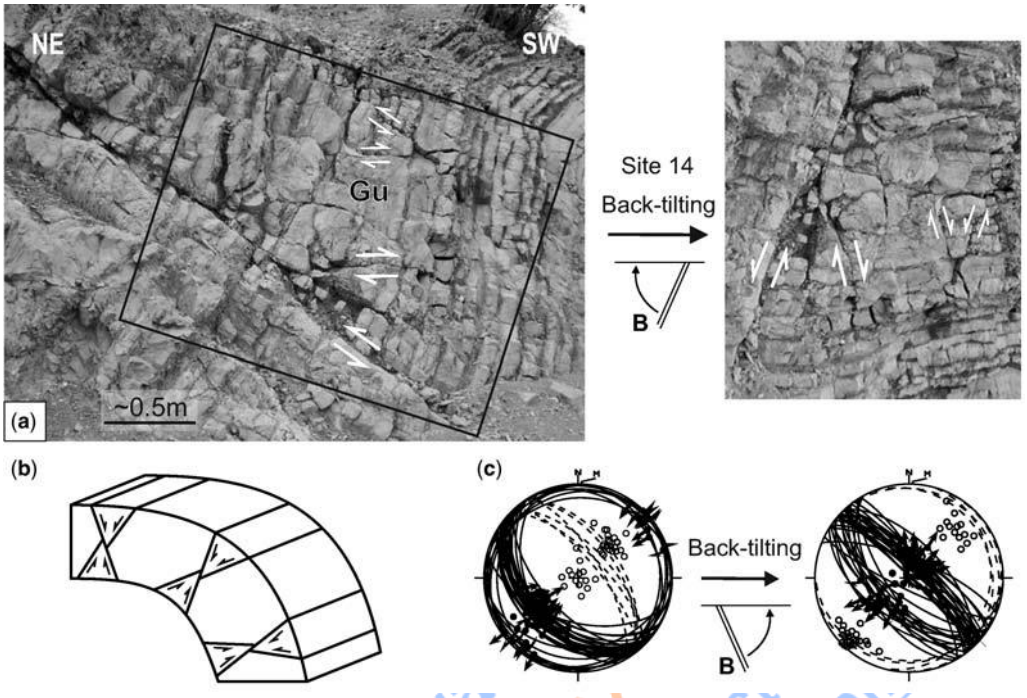

Fig. 5. Pre-folding conjugate normal faults within the upper Cretaceous sedimentary layers, indicating an extension that occurred between the late Cretaceous sedimentation and the middle Cenozoic folding. (a) Conjugate reverse faults in the present-day folded strata of the Gurpi Formation (Gu) at site 14 (left), interpreted as pre-folding conjugate normal faults by back-tilting the strata to an initial horizontal attitude (right). (b) Schematic illustration of pre-folding conjugate normal faults in different positions within folded strata, characterizing a uniform pre-fold extension. (c) Back-tilting presentation for the fault slip data of site 14. In the stereoplots, faults are shown by great circles, including the striae as indicated by filled circles and slip arrows. Dashed great circles are bedding planes. Isolated filled and open circles are poles to bedding and faults, respectively. Stereoplots are Schmidt (equal area) projections of the lower hemisphere, including the position of magnetic north (marked by small M).

slip data reveals the same north – south and NE – SW directions for the extensional s_3 stress axes, with similar average trends of N007E and N036E, respectively, in a pre-fold attitude (Fig. 8). Such a similarity in the results led us to infer that even in the absence of syntectonic sedimentation these pre-folding normal faults can also be considered as Mesozoic brittle structures.

The regional relationship between these two directions of extension and the general trend of the fold-and-thrust belt indicates that the north – south extension is oblique to the present NW – SE structural grain of the belt, whereas the NE – SW extension is perpendicular to it (Figs 7 & 8). A comparison between the two extensional stress trends shows that the north – south direction prevails among the syndepositional extensions (Fig. 7a). In contrast, the NE – SW direction dominates among the pre-folding extensions with no syntectonic sedimentation (Fig. 8a). This could be because in many cases the syndepositional normal faults probably reveal an older extension (see Table 1). The brittle structures related to these two major directions of extension are distributed throughout the entire study area in the HZB of interior Fars and each direction cannot be referred to a specific area. Examining the age of the affected rocks reveals that both populations of the normal faults developed partly contemporaneously during the Mesozoic era and do not belong to a distinct time span.

A minority of the Mesozoic syndepositional brittle structures (15%) comprise normal faults trending NNE – SSW, indicating a NW – SE extensional direction (sites 24, 43 and 76 in Fig. 7). Such an association between synchronous major and minor orthogonal normal faults can be interpreted as indicating the existence of cross-faults that separate different lateral blocks in the hanging wall of the major normal faults (Laubach & Marshak 1987). The coeval activity of the two

orthogonal fault sets can also be interpreted as indicating the existence of a regional biaxial extension, creating chocolate-tablet structures. Such a mechanism has already been identified by field evidence of normal faulting (Angelier & Bergerat 1983) and numerical modelling (Hu & Angelier 2004). However, such evidence of syndepositional NW–SE Mesozoic extension is very sparse in the study area relative to the other major north–south and NE–SW extensions and cannot be interpreted as indicating a distinct tectonic event.

Geometry of the Mesozoic structures

In the study area, the two calculated Mesozoic directions of extension are obtained from two sets of normal faults, displaying consistent average strikes of *c.* N098 and *c.* 135, resulting in an acute angle of *c.* 37 between these two trends (Fig. 9a). This combination of differently trending normal faults is well demonstrated by major structures in the geological map of Arsanjan, to the NE of Shiraz (Fig. 9b; GSI 2001*a*). These major normal structures are situated in the transition area between the Turonian iron-stained carbonate platform of the NEAPM and the deep-sea radiolarian sediments of the Neo-Tethyan oceanic basin (see Haynes & McQuillan 1974). Some of the normal faults of these two subsets have preserved their initial normal situations whereas others have been reactivated as reverse (Fig. 9c) and/or strike-slip faults (Fig. 9d) (see also Navabpour *et al.* 2006, 2007*a*). More precise regional fault slip observations were made to determine the possible relationship between these structures. It was thus revealed that successive striae are well preserved on some of the NW–SE faults, indicating two separate dip-slip and oblique-slip normal vectors (Fig. 10a, b). Further data analysis led us to separate and distinguish three kinds of fault slip movements (Fig. 10c): (1) dip-slip normal faults trending east–west; (2) dip-slip normal faults trending NW–SE; (3) oblique-slip sinistral normal faults trending NW–SE.

In the first case, the normal faults with east–west strikes are observed as conjugate brittle structures that dip north and south. Dip-slip fault striations with rake angles (R) greater than 70 on these fault planes indicate a north–south extensional stress regime, with horizontal σ_3 and σ_2 stress axes and vertical σ_1 axis (Fig. 10c, top). We could not find other successive normal striations on these fault surfaces. In the second case, dip-slip fault striations with R 70 also exist on conjugate NW–SE normal faults, indicating a NE–SW extensional stress regime with the same attitudes for the stress axes but different trends for σ_3 and σ_2 axes; most of the faults (*c.* 70%) dip to the NE (Fig. 10c, middle). The third case resembles the second one, but with oblique striae (R 70) on the same faults, indicating successive slips. The fault slip data thus show an oblique-slip sinistral normal faulting, indicating a transtensional stress regime with an approximately north–south direction of extension; most of the faults (*c.* 75%) dip to the NE, as before (Fig. 10c, bottom; note the inclined attitudes of σ_1 and σ_2 stress axes in the transtensional stress regime). Although the three fault slip subsets are separated based on stress tensor analysis of successive fault striations, the age relationship between the different normal faults remains unclear. In comparisons between sites, shifts in the chronology commonly occur. At some sites, the dip-slip movement occurred before the oblique-slip one (Fig. 10a), but at some other sites the relative chronology is opposite (Fig. 10b).

A further and major problem in our study resulted from the existence of local extensions induced by folding during the late Cenozoic era. For this reason, our conclusions regarding the Mesozoic extension were drawn from only the Mesozoic outcrops where evidence of syntectonic sedimentation could be found. We could not find systematic sedimentary evidence associated with normal faulting revealing a consistent regional syndepositional extension during the Cenozoic basin evolution of the study area. However, some local syndepositional normal faulting affected the Eocene Pabdeh marls in the southern rim of the HZB of interior Fars (North Sepidan, Fig. 11), indicating a possible extensional activity of the HZF during the early Tertiary period. Unfortunately, the related brittle structures were too few to allow an acceptable stress tensor analysis and to draw a firm conclusion. Our field observation suggests a NNW–SSE strike for this faulting, indicating an ENE–WSW direction of extension. Further studies are needed to evaluate the importance and significance of such an early Tertiary extension.

Age of the extensional events

Almost all the evidence suggests that the first stage of the Neo-Tethyan opening started by a rifting process between the Iranian and Arabian continental plates during Permian–Triassic times. This extensional event is documented by some Permian amygdaloidal basaltic flows in the HZB (Thiele *et al.* 1968; Berberian 1977). The seismic profile analyses across the Dezful Embayment have revealed that the Permian–Triassic sedimentation was related to the hanging wall of a normal fault (Fig. 12a; Sepehr & Cosgrove 2004), characterizing a synrift structure. Syndepositional conjugate normal faults are also observed in the Permian carbonate platform of Oman, south of the Hormuz Strait, where the tilted

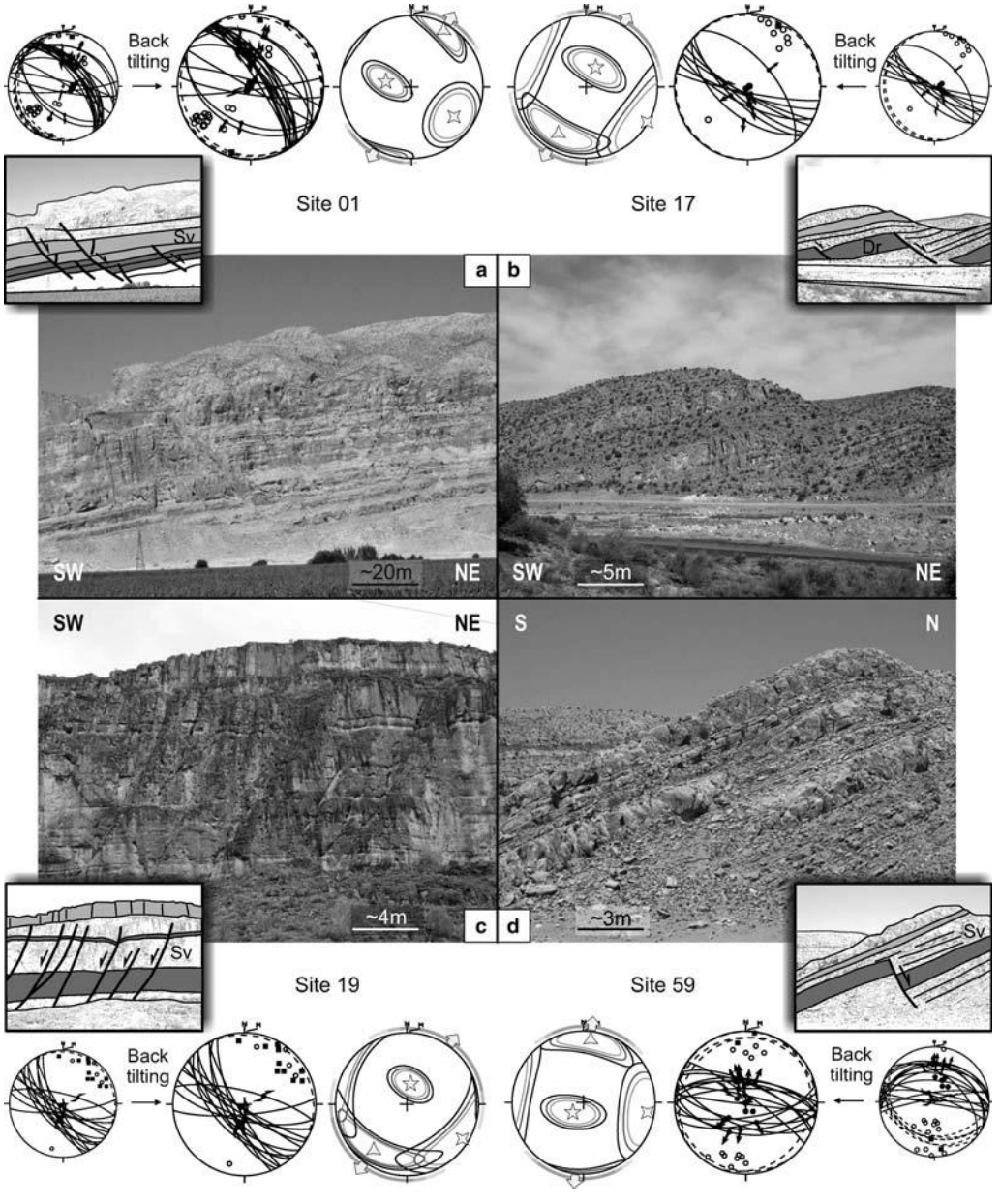

Fig. 6. Field evidence of syndepositional faulting within the Mesozoic sedimentary sequence, based on the situations observed at sites 01, 17, 19, 36, 55, 59, 77 and 79, indicating normal fault blocks associated with thickness change of coeval sediments (a) that are covered by non-faulted strata (b, c, d, g and h) and syntectonic sedimentary wedges (e and f). The related fault slip patterns and stress tensor determinations are included, indicating two major north – south and NE – SW direction of extension. Dr and Kn, Dariyan and Khaneh Kat Formations; Rd, radiolarite unit (note the unaffected layers on the right side of the photograph at site 79). In the stereoplots, small filled squares are poles to the tension cracks; stars with 5, 4 and 3 points mark the principal stress axes of σ_1, σ_2 and σ_3 respectively, with their 60, 75 and 90% confidence ellipses. Large open arrows show directions of extension with azimuthal confidence in grey curves. Other symbols and descriptions as in Figures 4 and 5.

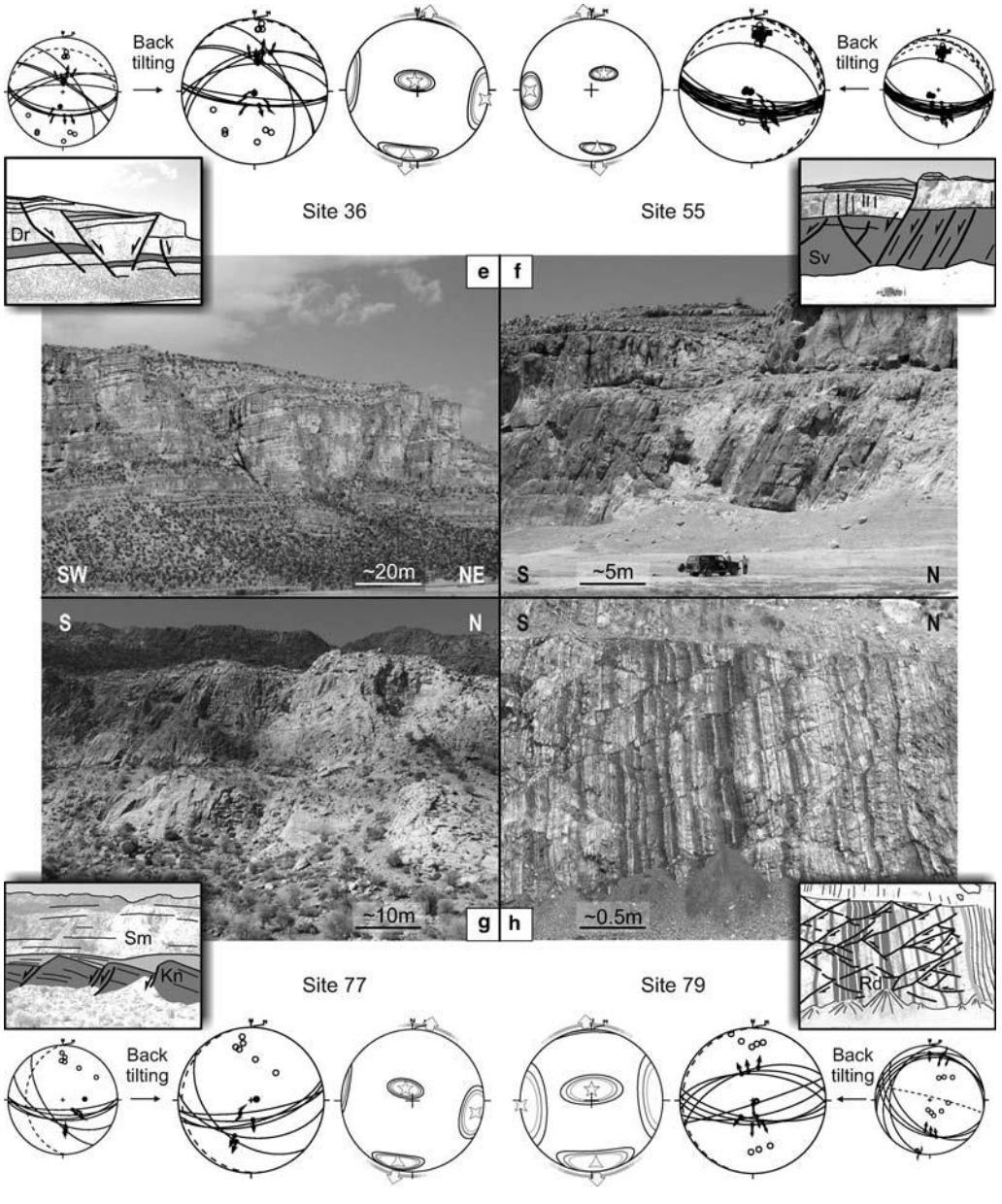

Fig. 6. (*Continued*)

blocks are sealed by an unconformity associated with dolomitization (Chauvet ***et al.*** 2004). These structures indicate a north – south direction of extension in the middle Permian period. We cannot discuss the Permian and Triassic extensions in the HZB, because the outcrops were scattered and not good enough for data collection. However, a late Triassic extension could be identified in the Khaneh Kat Formation, east of Shiraz (site 77, Fig. 6).

Leeder & Gawthrope (1987) have discussed the tectonostratigraphic evolution of a half-graben structure in coastal environments. They have shown how the uplifted footwall and downthrown hanging wall of the tilted blocks can be related to local erosion and facies changes in shallow-water

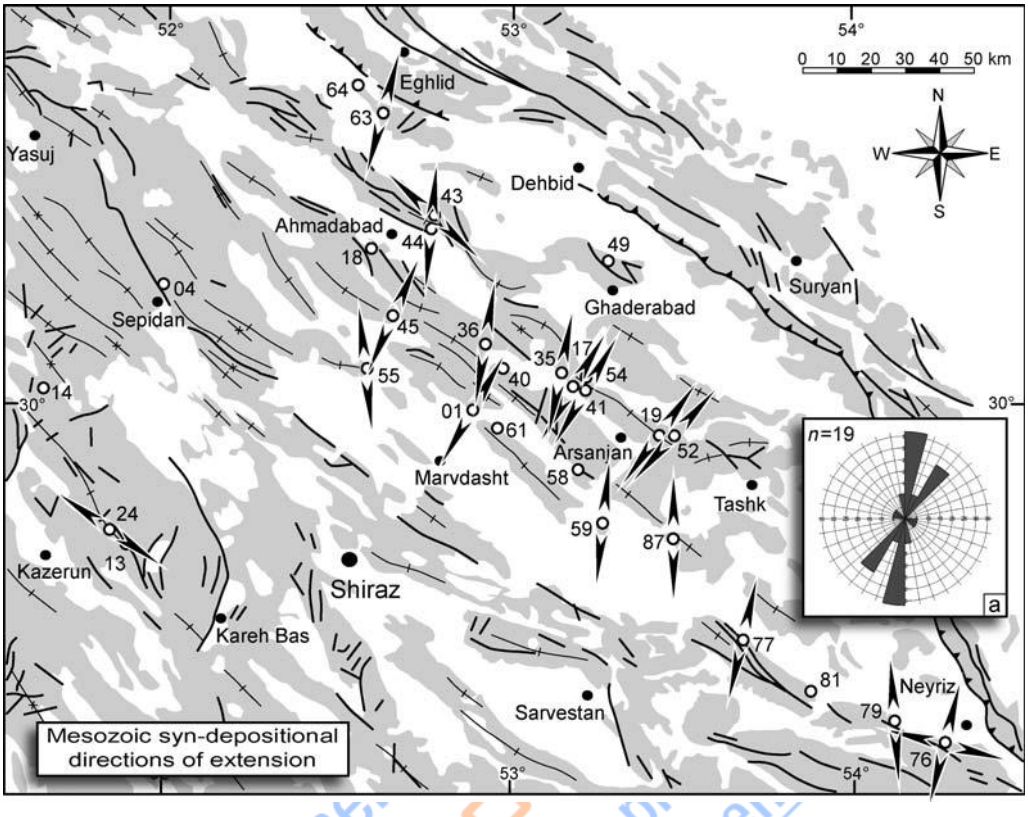

Fig. 7. Distribution map of the reconstructed s_3 stress axes (pairs of divergent black arrows), for extensional stress regimes obtained from the Mesozoic syndepositional normal faults throughout the study area. Inset (a) shows a rose diagram of s_3 stress axes (n ¼ 19), indicating two distinct north – south and NE – SW directions of extension with average trends of N0068 and N0348. Geological details are shown in Figures 2 and 3, and listed in Table 1.

conditions, respectively. Such a condition has already been reported from the top of the Sarvak Formation in SE Zagros at Kuh-e-Faraghun, where wedges of conglomerates were derived from adjacent normal fault scarps and were sealed by the overlying Palaeocene – Eocene sediments (Fig. 12b; Stoneley 1990). In our study area, we observed intraformational angular unconformities within the Sarvak Formation along approximately the middle axis of the HZB of interior Fars, associated with block tilting, syndepositional normal faults and brecciated facies in the upper parts of the Sarvak Formation (Figs 4b and 12c – f). This evidence can be correlated especially along the major normal fault blocks of the Turonian – Early Coniacian in the Arsanjan area, reconstructed by geological observations of Stoneley (1981).

Most of the syndepositional normal faulting and tilted blocks that we could determine occurred in the Middle – Upper Triassic (Khaneh Kat Fm), Middle – Upper Jurassic (Surmeh Fm), Aptian (Dariyan Fm), Cenomanian – Turonian (Sarvak Fm) and Campanian – Maastrichtian (Gurpi Fm) sedimentary rock units (see Table 1). As mentioned above, there are some reported Mesozoic angular unconformities from sedimentary sequences of Late Triassic (Szabo 1977; Szabo & Kheradpir 1978), Late Jurassic (Murris 1978), Aptian – Albian (James & Wynd 1965; Setudehnia 1978), Late Turonian (Haynes & McQuillan 1974) and Late Maastrichtian (James & Wynd 1965; Setudehnia 1978) age (see Fig. 3). Most of these unconformities have been reported from the HZB and were associated with intraformational conglomerate, breccia, glauconitic sandstone and iron-stained dolomitic shelf carbonate.

A good correlation thus is obvious between the angular unconformities and syndepositional extensional structures within the Mesozoic stratigraphic sequence of the HZB, when we examine their ages in a correlation chart (Fig. 13). This correlation becomes more acceptable when is compared with

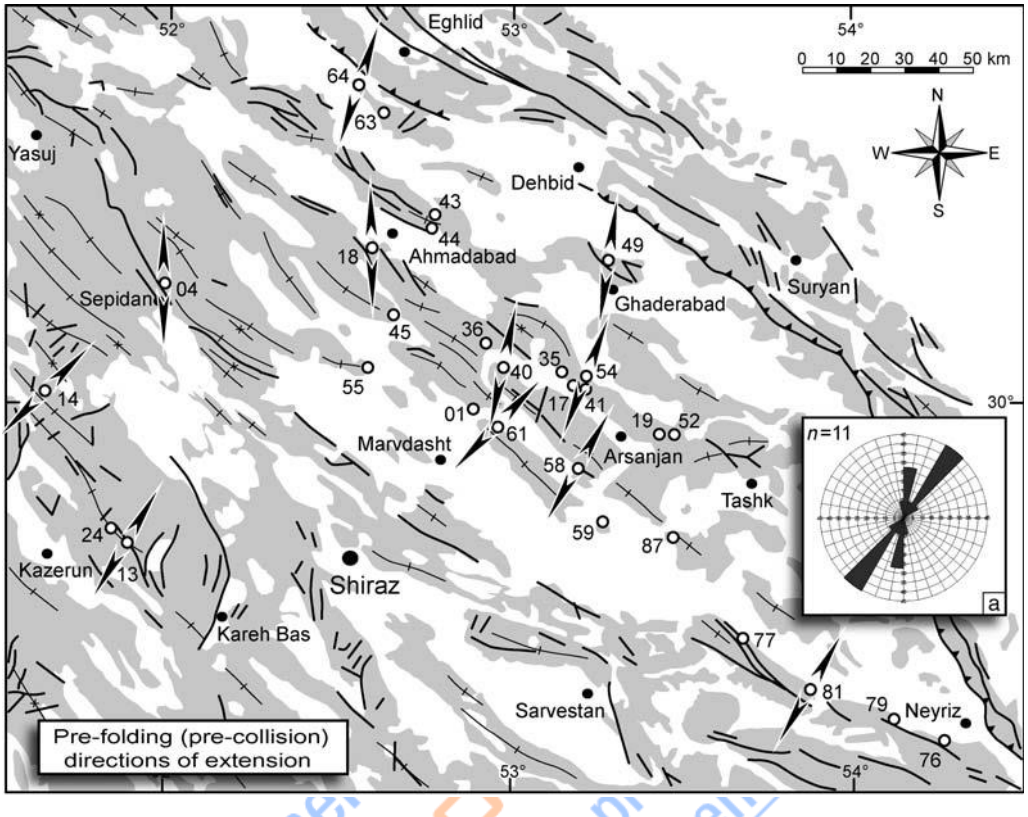

Fig. 8. Distribution map of the reconstructed s_3 stress axes for extensional stress regimes obtained from back-tilted Mesozoic strata with no evidence of syntectonic sedimentation, indicating extensions that occurred before the late Cenozoic folding. Inset (a) shows a rose diagram of s_3 stress axes (n ¼ 11), indicating two distinct north – south and NE – SW directions of extension with average trends of N0078 and N0368, similar to that of the syndepositional structures (see Fig. 7). Arrows as in Figure 7. Geological detail are shown in Figures 2 and 3, and listed in Table 1.

the subsidence rates of the ZSFB of Fars Arc, based on formation isopach maps. According to Bordenave & Hegre (2005), an average background apparent subsidence rate of *c*. 10 m Ma^{21} within the ZSFB of Fars Arc was increased to about 30, 25, 60 and 20 m Ma^{21} during the deposition of the Khaneh Kat, Dariyan, Sarvak and Gurpi – Pabdeh Formations, respectively (Fig. 13). However, the successive angular unconformities of the HZF were not reported from the ZSFB. This situation indicates that the inner parts of the NEAPM were more stable to the SW of the HZF than to the NE. We thus infer that most of the reported unconformities within the Mesozoic sedimentary sequence of the HZB could have been related to a contribution of both the block tilting and the basin deposition or erosion processes in the northeastern rim of the NEAPM, suggesting successive episodes of extension that have been recorded as brittle structures during the continuous subsidence. This aspect of unconformities related to block tilting was also illustrated in the North Sea basin (Kyrkjebo ***et al.*** 2004) and in the Neo-Tethyan passive margin of both the North Anatolian Palaeorift (Kocyigit & Altiner 2002) and Oman (Chauvet ***et al.*** 2004).

According to our data, there is little evidence of a syndepositional normal faulting within the Eocene marls of the Pabdeh Formation (see Figs 11 & 13). It has been reported that outcrops of the Eocene rocks have been subjected to subaerial weathering (James & Wynd 1965; Motiei 1993), because of uplifting and folding along the northeastern rim of the ZSFB during the late Eocene – early Oligocene epochs (Hessami ***et al.*** 2001). New field observations confirmed that the onset of collision occurred in the late Oligocene – early Miocene epochs (Agard ***et al.*** 2005, 2006) and that the folding started in the early Miocene epoch (Sherkati ***et al.*** 2005). A dramatic increase in subsidence rate, to more than 140 m Ma^{21}, is evidenced in the

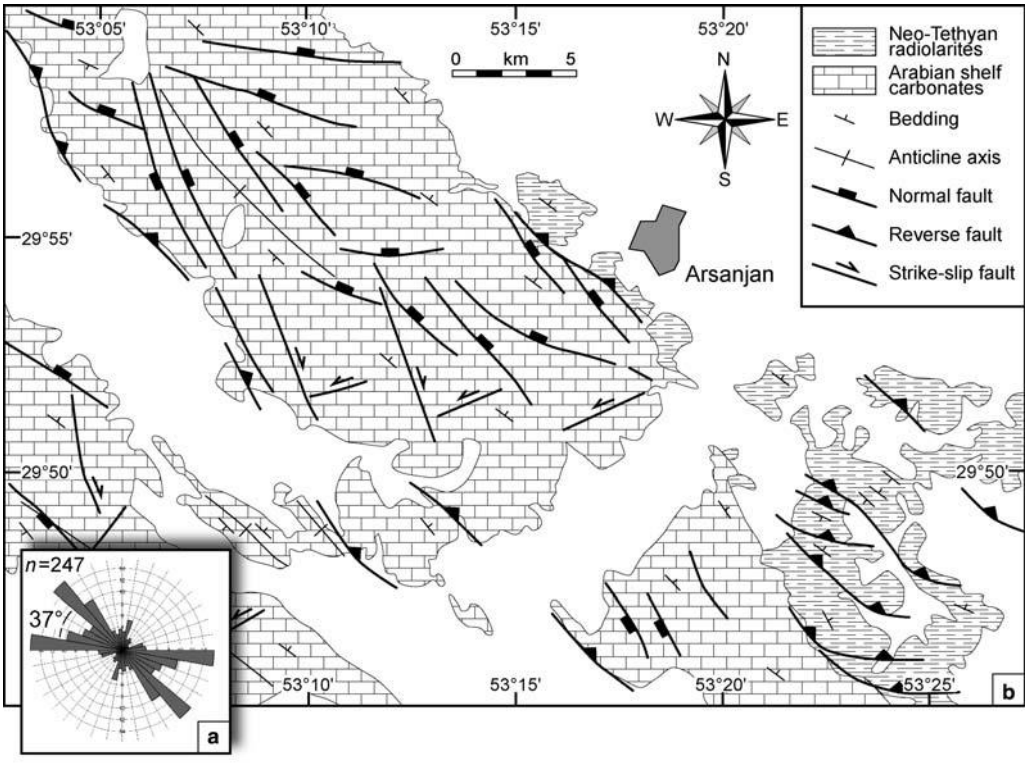

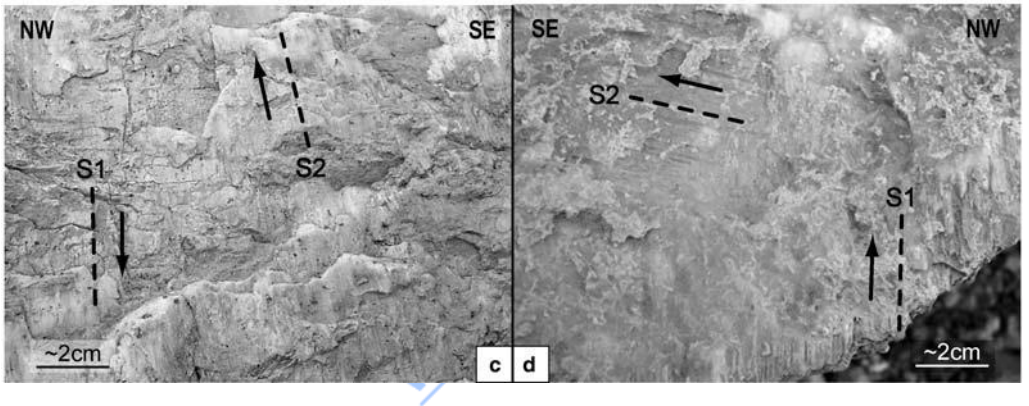

Fig. 9. Regional attitudes of the Mesozoic normal faults. (a) Rose distribution of the strikes of the Mesozoic normal faults throughout the study area (*n* ¼ 247), revealing two main *c*. N098 and *c*. N135 trends at an acute angle of *c*. 37. (b) Structural map of the Arsanjan area (redrawn from GSI 2001*a*), indicating two east–west and NW–SE strikes of the Mesozoic major normal fault sets that dip mainly to the north and NE throughout a gentle anticline. Location is shown as in Figure 2. (c) Reverse reactivation on a pre-existing Mesozoic normal fault within the Gurpi Formation. S1 indicates a normal fault slip vector that is characterized by old striae grooved on the fault surface; S2 indicates a reverse fault slip vector that is characterized by fresh calcite steps. (d) Successive reverse and strike-slip reactivation on a high-angle fault within the Sarvak Formation, S1 then S2 respectively, indicating a change in stress state during the late Cenozoic collisional process (see Navabpour *et al*. 2006, 2007*a*).

Oligocene epoch during the deposition of the Asmari Formation in the ZSFB of the Fars Arc (Fig. 13; Bordenave & Hegre 2005). Considering these ages, it may also be inferred that the subaerial weathering of the Eocene rocks could have been a result of extensional tectonics and block tilting, as

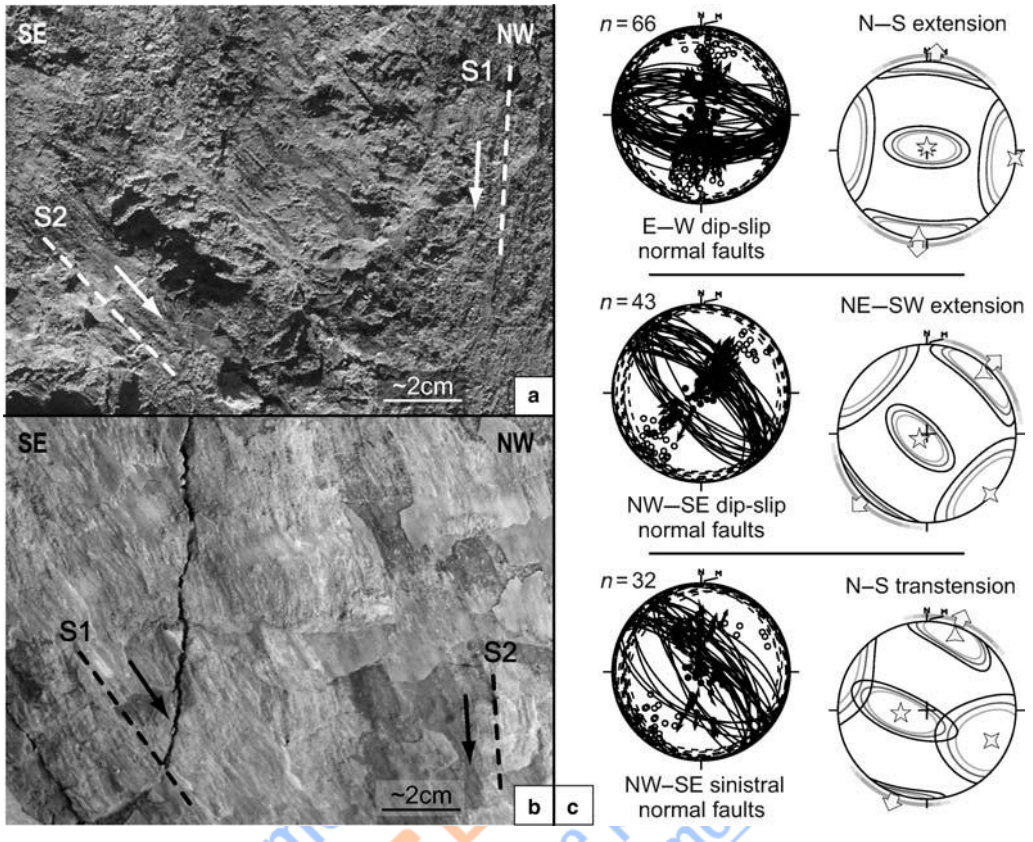

Fig. 10. Major normal fault slip geometries within the Mesozoic units of the HZB. (a, b) Successive striae on a fault plane, S1 then S2, indicate two different relative fault slip chronologies. This situation implies that no systematic succession of movements can be characterized between dip-slip and oblique-slip sinistral normal fault slips. (c) Three normal fault geometries separated based on different strikes, rakes of striae and stress tensor determination at different sites throughout the study area: east – west normal faults indicating a north – south extension (top), NW – SE normal faults indicating a NE – SW extension (middle), and NW – SE sinistral normal faults indicating a transtensional north – south extension (bottom). Number of fault slip data, ***n***, shown at top left corner of each diagram. Symbols of stereoplots as in Figures 5 and 6.

is described above for the Mesozoic units. Such an interpretation would indicate that the Mesozoic syndepositional history of extension and block tilting of the NEAPM probably continued during the early Cenozoic era, prior to the continental collision. Further studies would be essential to indicate if such view is correct. After the onset of collision, the angular unconformities of the middle – late Cenozoic stratigraphic sequence characterize the different folding episodes of the Zagros basin (Sherkati ***et al.*** 2005).

Discussion

In contrast to brittle tectonic analysis in the tabular areas of plate interiors, our study in the HZB required careful consideration of relationships between the brittle structures and folds. This interaction between brittle structures and folds results in structural complexity. In particular, the number of stress regimes reconstructed in the present-day structure is larger than the number of tectonic events that occurred in the Mesozoic history of the HZB, because of the reactivation of inherited faults and the presence of brittle structures related to the late Cenozoic compressional stress fields. However, numerous observations of syndepositional normal faulting related to the Mesozoic history of the study area facilitated deciphering of the tectonic relative chronology. Similar aspects of syndepositional normal faulting have already been highlighted for the HZB of Kermanshah (Angelier ***et al.*** 2006), the HZB of

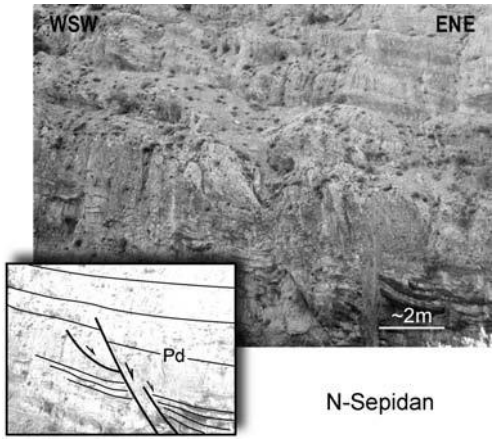

Fig. 11. Syndepositional evidence of normal faulting in the Eocene Pabdeh marls (Pd) in the southern rim of the HZB (N Sepidan; see Fig. 2 for location map), indicating a possible extensional activity of the HZF during the early Tertiary period, prior to the continental collision.

interior Fars (Navabpour *et al.* 2006) and in the northern North Sea along the Norwegian continental shelf (Nottvedt *et al.* 1995).

The brittle tectonic analysis and palaeostress reconstructions presented in this study bring new approaches to the study of the tectonic evolution of the former NEAPM in the Zagros collisional belt. However, questions remain regarding some natural limitations of the methods. For instance, small outcrops of the Palaeozoic and Triassic sedimentary rocks do not provide sufficient information about the Permian – Triassic rifting and oceanic opening process that are recorded within the NEAPM, as was reported from the Permian carbonate platform of Oman by Chauvet *et al.* (2004). The quality of fault slip striae preserved on the Mesozoic faults is not often good enough to allow identification of clear relative chronologies between the various Mesozoic tectonic events. In addition, Cenozoic outcrops are few in the HZB of interior Fars, which makes identification of possible syndepositional tectonic activities in the early Cenozoic sedimentary basin difficult.

In this section, we intend to discuss the Mesozoic extensional stress regimes and to reconstruct a possible structural model for the Mesozoic brittle tectonic evolution of the HZB, considering regional tectonic aspects. To this end, we considered the stratigraphic ages of syndepositional normal faulting (see Figs 6 & 7) and the maximum stratigraphic ages that can be assumed for the reconstructed prefolding extensional events (see Figs 5 & 8; see also Table 1 for a complete account). It was thus possible to plot the age of the events as a function of the extensional directions revealed by the inversion of fault slip data (Fig. 14). The resulting distribution clearly shows the two main north – south and NE – SW directions of extension (Fig. 14a), as already illustrated by the rose diagrams of reconstructed σ_3 stress axes based on the Mesozoic and prefolding normal fault slip data (see Figs 7a & 8a). It also shows that these two directions of extension correspond to roughly different time intervals, *c.* 240 – 90 Ma for the north – south extensional trend and 180 – 60 Ma for the NE – SW extensional trend (Fig. 14b). It is interesting to note that both the directions of extension coexisted during the period of 180 – 90 Ma (marked as the light grey area in Fig. 14b).

This approach indicates a possible gradual regional change in direction of extension from north – south to NE – SW. In other words, it seems that the direction of extension has changed slightly from a margin-oblique trend to a margin-perpendicular one, during the Mesozoic history of the NEAPM. First, margin-oblique extension occurred during the Triassic – early Jurassic period. The margin-perpendicular extension then prevailed over the area during the late Jurassic – Cretaceous period, whereas the margin-oblique one continued until the middle Cretaceous period. The existence of such a continuous extension and a possible gradual change in stress direction during the Mesozoic era, as well as the similarities between the trends of the corresponding normal faults and the late Ceno- zoic reverse structures, encouraged us to search for possible explanations.

Existence of an oblique crustal stretching?

The geometry of fault systems of a rift zone reflects whether it evolved in response to orthogonal or oblique divergence of its flanking stable blocks (Tron & Brun 1991). A classical example of oblique crustal stretching is the western branch of the East African rift system (Rosendahl *et al.* 1992). It should also be kept in mind that during the evolution of a rift the stress regime governing its development may significantly change. The structural pattern of the northern margin of the Aden Gulf presents two differently oriented normal fault systems that were generated on the continental margin under an oblique extensional stress regime (Huchon & Khanbari 2003). The strikes of the normal faults are parallel to the trend of both the oceanic spreading axis and the continental margin, indicating an acute angle of about 40° between the fault trends (Fig. 15a). Creating a mirror view of the Aden Gulf structures (Fig. 15b) and comparing it with the Mesozoic extensional structures of the HZB (Fig. 15c), the question of the history of the NEAPM arises: has it undergone two differently

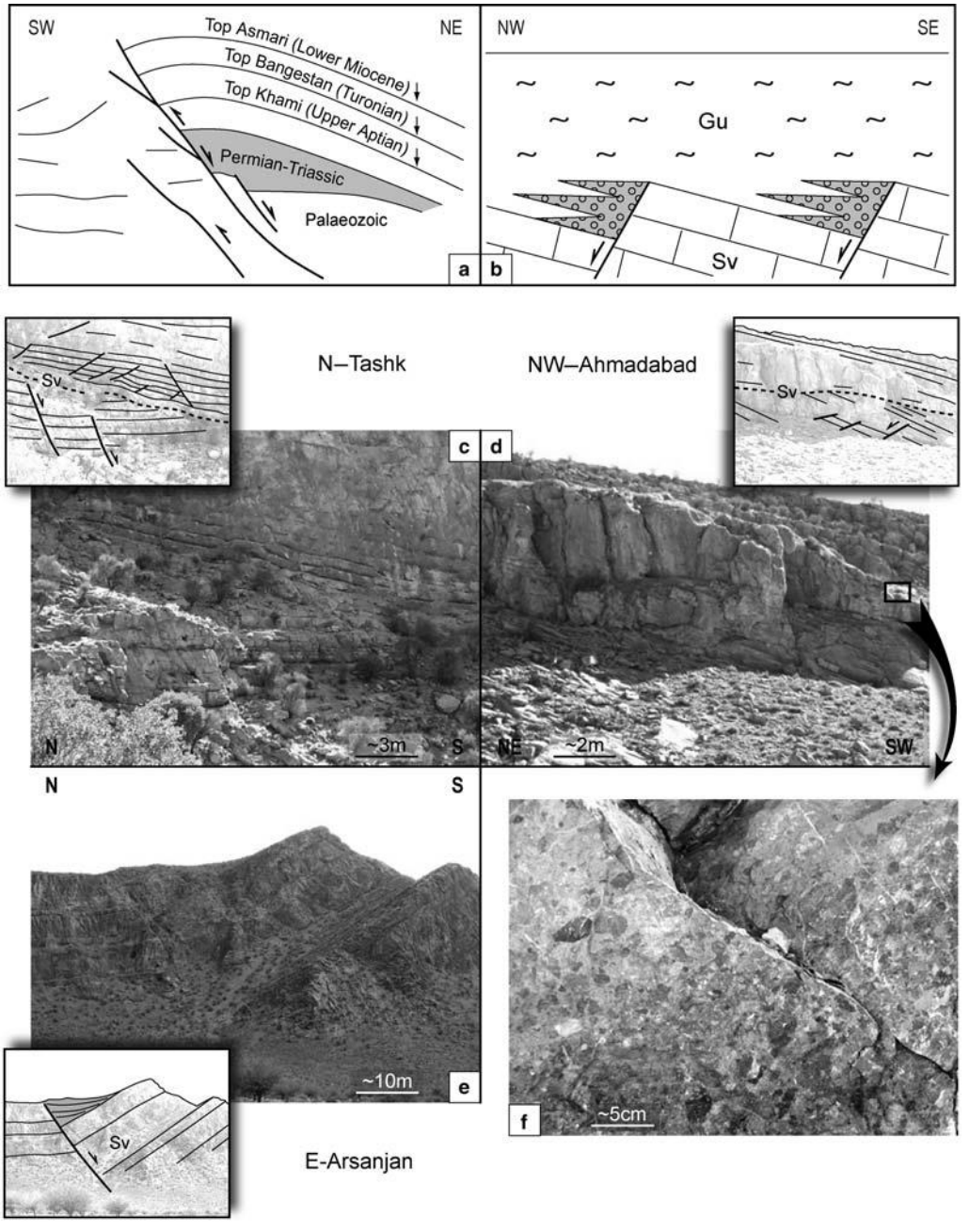

Fig. 12. Aspects of syndepositional extensional structures within the Zagros basin. (a) Permian – Triassic strata (in grey) that are involved with the hanging wall of a buried normal fault inverted during the late Cenozoic folding, based on seismic profile analysis across one of anticlines of the Dezful Embayment (redrawn from Sepehr & Cosgrove 2004; see Fig. 1 for location map). (b) Intraformational conglomerate and breccia (in grey) related to normal faulting within the sedimentary basin of the Sarvak (Sv) and Gurpi (Gu) Formations in SE Zagros at Kuh-e-Faraghun during the Turonian – Coniacian (redrawn from Stoneley 1990; see Fig. 18a for location map). (c, d) Intraformational angular unconformities (dashed lines) associated with normal faulting within the Sarvak Formation. (e) Extensional block tilting associated with syndepositional sedimentary wedge (in grey) within the Sarvak Formation. (f) Brecciated facies of the Sarvak Formation mainly observed at the upper parts above the intraformational unconformities. (See Fig. 2 for localities.)

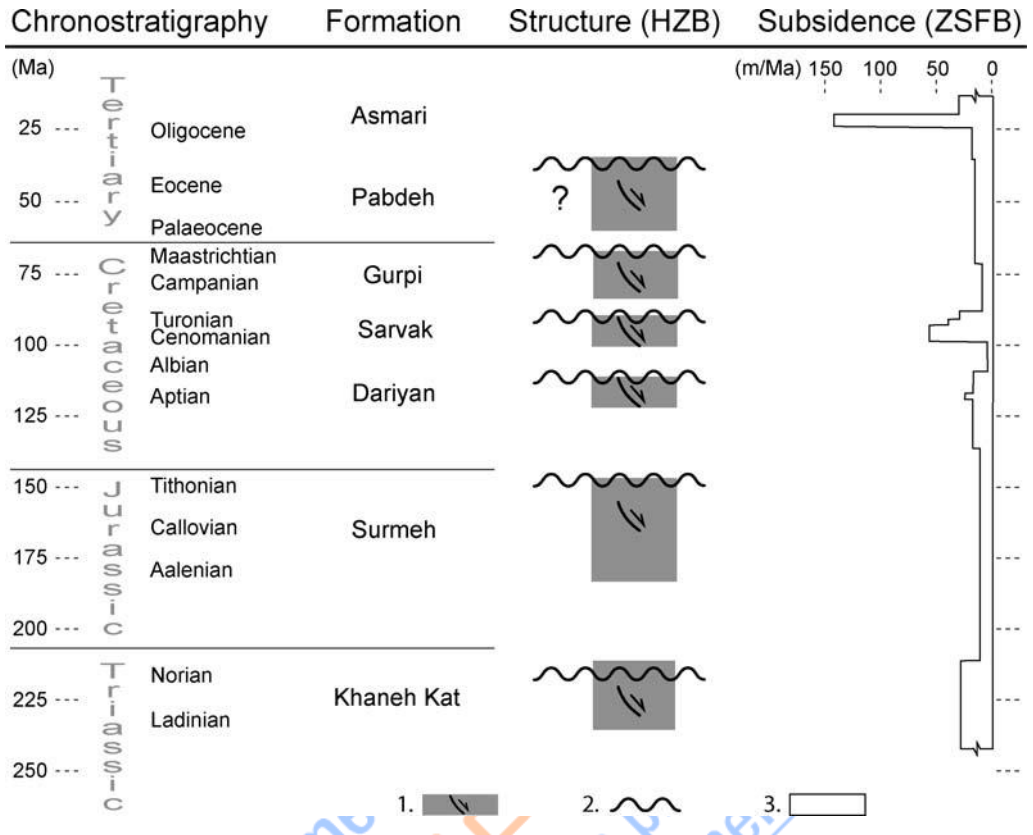

Fig. 13. Correlation chart for syndepositional normal faulting and unconformities of the HZF of interior Fars and apparent subsidence rates of the ZSFB of the Fars Arc for the Mesozoic – early Cenozoic time interval. 1, Rock unit associated with syndepositional normal faulting; 2, angular unconformity (references in the text and Fig. 3); 3, apparent subsidence rate (i.e. the ratio between thickness of the sedimentary rock unit and the duration of its deposition) from Bordenave & Hegre (2005).

oriented far-field crustal extensions, or have the structures resulted from different local phenomena under a single far-field extension? If we assume that two differently oriented far-field extensional tectonic events have affected the region, each related structure should be referable to a specific time span, and a clear chronology should emerge between these extensional tectonic regimes. A general change in the direction of extension certainly occurred during the Mesozoic era, but as shown by our data this change was gradual and both the different normal fault movements and the related north – south and NE – SW extensional directions occurred contemporaneously during middle Jurassic – middle Cretaceous times (Fig. 14b).

On the other hand, the Mesozoic syndepositional extensional brittle structures of the HZB of interior Fars developed within the sedimentary cover of the NEAPM after the Permian – Triassic rifting. Some additional information on the basement structures is necessary to simulate a possible structural evolution of the Permian – Triassic rifting. In most cases, the direction of a single segment of an oceanic ridge does not change significantly with respect to the corresponding continental margin segment during sea-floor spreading, because of the rigidity of the oceanic crust. A study of a frozen mantle flow structure in the Neyriz ophiolitic complex revealed the existence of a palaeo-oceanic spreading centre with a reconstructed axis trending N1058, compati- ble with the geometry and orientation of harzburgite foliations and lineations and sheeted dykes (Fig. 15d; Nadimi 2002). Although such a structure could have been involved with differential changes in direction during the late Cretaceous ophiolite obduction, it strikes almost parallel to the strike of syndepositional normal faults within both the Neyriz radiolarites and the Mesozoic sedimentary sequence of the NEAPM that revealed the north – south margin-oblique extension throughout the study area (see

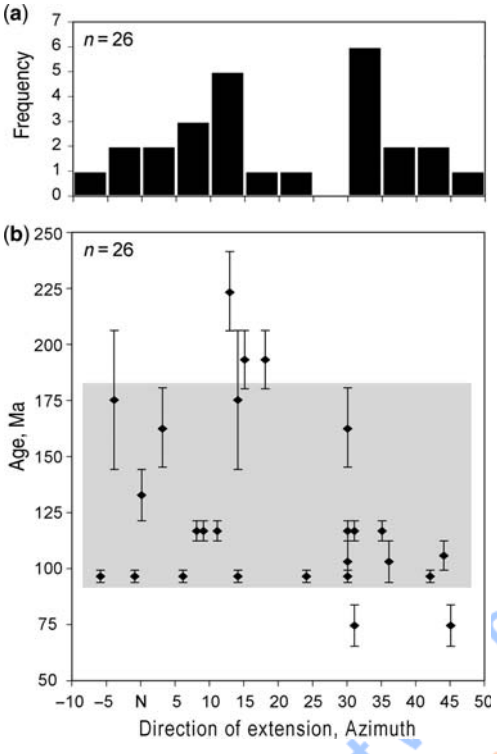

Fig. 14. Relationships between age, trend and frequency of the Mesozoic extensions. (a) Frequency – direction relationship for the extensional stress trends (n ¼ 26), representing the main north – south and NE – SW directions (see Fig. 7). (b) Age – direction relationship for the extensional events, suggesting a general change in the direction from roughly north – south to NE – SW during the Mesozoic era. Vertical bars show the age range of the corresponding lithostratigraphic unit in which normal faulting was observed. The time overlap of the two directions for the period of 180 – 90 Ma ago is marked by the light grey area.

Figs 6, 7 & 9a). This situation indicates that no major differential change in structural orientation occurred during the late Cretaceous ophiolite obduction, suggesting a possible obliquity between the Neo-Tethyan palaeo-oceanic ridge and the NEAPM.

The existence of such a possible obliquity led us to infer that the coeval bidirectional Mesozoic extension could have originated by gravitational reactivation of similar structures within both the Palaeozoic sedimentary sequence and the continental basement similar to that of the Aden Gulf, characterizing a Permian – Triassic oblique crustal stretching. By adopting the results of experimental oblique extensional modelling of Tron & Brun (1991) for the present-day situation of the observed extensional structures in the HZB of interior Fars (Fig. 15c), we assume an oblique rifting under a far-field north – south extensional stress trend at a stretching angle of 608 (Fig. 16a). In such a transtensional condition, two sets of normal faults could have been formed within the stretched continental crust parallel to both the divergent flanks and the oblique spreading axis, trending NW – SE and east – west respectively within the present-day geographical reference frame, with an acute angle of 308 between the fault trends. Whereas Mesozoic normal faults are well documented within the sedimentary cover of the HZB of interior Fars (Navabpour *et al.* 2006; this study), there is unfortunately no seismic evidence to reveal the existence of such structures within the basement of the study area. However, further to the south, considerable seismic activity throughout the ZSFB of the Fars Arc has revealed the existence of active reverse faults (Berberian 1995; Gillard & Wyss 1995) within the basement (Maggi *et al.* 2000; Talebian & Jackson 2004; Engdahl *et al.* 2006) (Fig. 16b; Table 2), based on consideration of earthquake focal mechanism solutions.

Adopting a half-graben structure for the NEAPM, we considered the NE-dipping nodal planes of the earthquake focal mechanisms as fault planes of the inherited rift structures. A statistical rose analysis of these fault planes (Fig. 16c) reveals two aspects that deserve attention. First, the strikes of the reverse faults indicate two major *c.* N0858 and *c.* N1208 trends for the basement inherited brittle structures, with an acute angle of *c.* 358 between these faults similar to that is expected from the oblique stretching model. Second, most of these faults show an average dip angle of *c.* 608, characterizing high-angle reverse faults (Berberian 1995), which is consistent with the usual continental normal faulting geometry. Therefore, we prefer to interpret the structural pattern of the present-day basement reverse faults together with the obliquity of the Neyriz palaeo-oceanic spreading centre as sufficient evidence supporting the Permian – Triassic oblique stretching model for the Neo-Tethyan opening. The consistency between the strikes of both the basement reverse faults of the ZSFB of the Fars Arc and the Mesozoic normal faults within the sedimentary cover of the HZB of interior Fars also provides indirect confirmation that no major horizontal block rotation has occurred between these domains during the evolution of the NEAPM and the subsequent Zagros collision.

Possible scenario for the Mesozoic extensions

A possible scenario has already been proposed for the oblique opening of the Aden Gulf, by Huchon & Khanbari (2003). Those workers have shown that the NE – SW extensional stress related to the

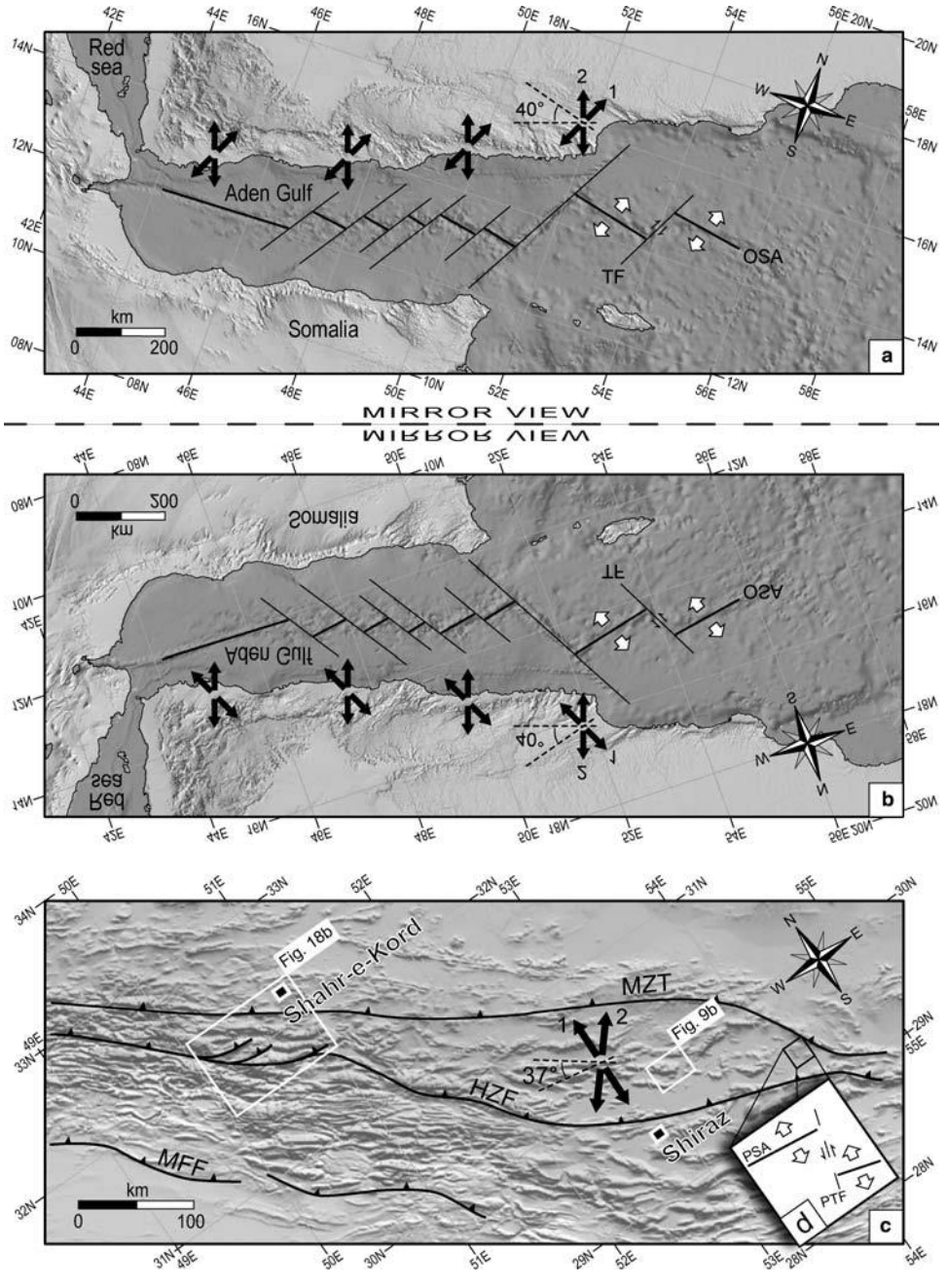

Fig. 15. Recent and ancient oblique extensional tectonics of the Arabian continental margins. (a) Recent active oblique opening of the Aden Gulf (redrawn from Huchon & Khanbari 2003). (b) Mirror view of (a) to be compared with (c). (c) Regional view of the reconstructed Mesozoic extensional trends of the former NEAPM in the HZB (see also Figs 7 – 9). (d) Inferred palaeo-oceanic spreading axes of the Neo-Tethyan basin within the ophiolites of the Neyriz area (redrawn from Nadimi 2002). OSA, oceanic spreading axis; TF, transform fault; PSA, palaeo-spreading axis; PTF, palaeo-transform fault. White and black pairs of arrows show far-field and near-field stress components, respectively. Numbers refer to relative chronology. Dashed lines show trends of normal faults. The acute angle between the two normal fault trends indicates a possible obliquity between the PSA and the former NEAPM. Location is shown in Figures 1 and 2.

active spreading axes of the Indian Ocean is oblique to the diverging east–west trend of the southern Arabian continental passive margins. This extensional trend is preserved on the continental margins as normal faults trending NW–SE and is replaced by a younger trend of an almost north–south extension perpendicular to the trend of the continental margins (see Fig. 15a). The north–south direction of extension was thus interpreted as the result of an eastward propagation of the oceanic spreading axis into the continental crust, following a mechanism similar to that of a tension crack but at lithospheric scale, which characterizes a rift-to-drift transition. Such a scenario may be sufficient to describe a similar process for evolution of the brittle structures within the Palaeozoic–Triassic sedimentary sequence during the Permian–Triassic Neo-Tethyan oblique opening between the Arabian and Iranian continental plates, as proposed earlier. However, there is still debate on the interpretation of the different syndepositional normal fault slip geometries of the HZB of interior Fars, especially the oblique-slip sinistral normal fault movements, during the Jurassic–Cretaceous history of the NEAPM long after the creation of the Neo-Tethyan oceanic environment. The structural pattern of the major Mesozoic normal faults could have been produced by gravitational reactivation of similar inherited structures within either the basement and/or the underlying Palaeozoic sedimentary sequence over the basal Infracambrian Hormuz Salt detachment (see Fig. 3).

It is known that at shallow levels the structural style of a rift is strongly influenced by the lithological composition of the down-faulted pre-rift and synrift sediments. Evaporitic rocks can give way to the development of multilevel extensional detachment faulting (Jarrige *et al.* 1990; Jarrige 1992) and can act as sole-out levels for secondary fault systems developing in response to gravitational instability (Nottvedt *et al.* 1995). Recent analogue modelling studies of Soto *et al.* (2007) indicated how different basin-bounding fault geometries and thickness of a viscous layer within the brittle pre-rift sequence influence the deformation and sedimentary basin patterns related to the half-graben extension. For a long time, it has been known that the Infracambrian Hormuz Salt Formation has behaved as a detachment layer controlling different structural styles of the folded sedimentary cover with respect to the faulted basement (Colman-Sadd 1978; Talbot 1979; Koyi *et al.* 2000; Sherkati *et al.* 2005; Sepehr *et al.* 2006). Such a thick detachment layer could have played an important role in the extensional Mesozoic history of the NEAPM as well. The relatively high subsidence rate (i.e. *c.* 60 m Ma^{21}) in the Fars Arc during the Cenomanian, which is marked by the brecciated facies and intraformational angular unconformities of the Sarvak Formation in the HZB (Stoneley 1981, 1990; this study), is attributed to readjustment of faulted blocks and gravitational movements on the basal salt detachment (Bordenave & Hegre 2005). This is consistent with the idea that the first gentle movements within the sedimentary cover, predating the development of the major late Cenozoic Zagros structures, probably triggered the salt plugs to well up (Player 1969; Kent 1970, 1979; Koyi 1988; Talbot & Alavi 1996). Regional extension is believed to be an important initiator of salt diapirs during thin- and thick-skinned stretching (Vendeville & Jackson 1992). It seems likely that the salt plugs pierced the thinned Palaeozoic sedimentary sequence along the HZF during the Permian–Triassic extension (Sepehr & Cosgrove 2004).

We infer that during the Permian–Triassic oblique continental stretching, the initial east–west normal faults could have been produced within both the basement and the Palaeozoic sedimentary cover under a north–south extensional stress field in the future HZB close to the rift axis, characterizing a thick-skinned extension (Fig. 17a). These east–west normal faults could be associated with the NW–SE normal faults further to the south in the future ZSFB on the NEAPM, as evidenced by the present-day seismicity of the basement struc- tures. Creation of the oceanic environment to the NE of the Arabian margin together with the role of the Hormuz Salt detachment then provided conditions for the sedimentary cover to undergo continuous extensional block tilting on the inherited east–west margin-oblique normal faults, with some localized oblique-slip and margin-parallel faulting, during Triassic–Jurassic times (Fig. 17b). The extensional tectonic regime then gradually changed and the NE-dipping NW–SE margin-parallel normal faults prevailed over the future HZB, deeply affecting the entire sedimentary cover to the basal detachment, characterizing a dominant thin-skinned extension. Such continuous extensional tectonics over a salt detachment layer has already been discussed for the structural evolution of the West African passive margin after the South Atlantic rifting (Marton *et al.* 2000). Meanwhile, the reactivation of the preliminary inherited east–west normal faults within the Palaeozoic rocks (possibly as a result of the Mesozoic sedimentary load) could have induced local north–south extensional stress trends beneath the Mesozoic sedimentary sequence. These localized north–south extensions could then result in initiation of the syndepositional earth–west normal faults and some sinistral reactivation on the NW–SE normal faults within the overlying sedimentary layers during the Cretaceous history of the NEAPM (Fig. 17c). Interestingly, the higher frequency of

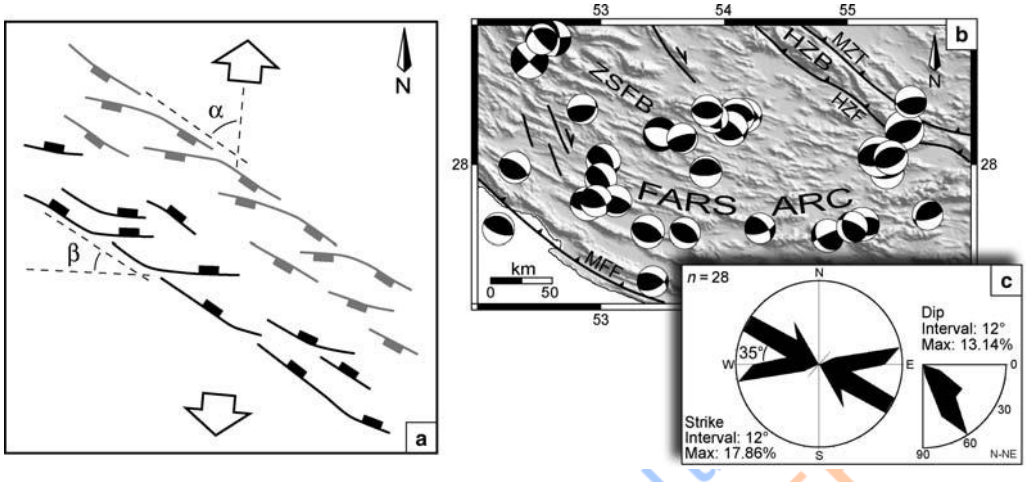

Fig. 16. Structural model of an oblique extension and basement structures of the Zagros. (a) Schematic illustration of a classical transtensional extension with a stretching angle of $\alpha = 60°$ (redrawn from Tron & Brun 1991). Adopting this model for the present-day geographical reference of the Zagros suggests an oblique half-graben structure composed of north- to NE-dipping normal faults (highlighted as black faults in the figure) trending east – west and NW – SE with an acute angle of $\beta = 30°$ between the fault trends. (b) Basement structures of the ZSFB of the Fars Arc revealed by earthquake focal mechanisms, most of which indicate reverse faulting (based on CMT database for 1976 – 2007 time interval; see Table 2), envisioned as inversion on the earlier normal faults (e.g. Jackson 1980). Considering the half-graben structure of the former NEAPM, most of the north- to NE-dipping nodal planes indicate high-angle (*c.* 60°) reverse faults (c) trending *c.* N085° and *c.* N120° with an acute angle of *c.* 35° between the fault trends. Location is shown in Figure 1.

the NE-dipping normal faults with respect to the SW-dipping ones (see Fig. 10c) characterizes the half-graben structure of the sedimentary cover of the NEAPM during the Mesozoic era, which is also evidenced by a micro-earthquake survey of the present-day active reverse faults within the basement of the ZSFB of the Fars Arc (see Tatar *et al.* 2004). It should be noted that the tectonic evolution may significantly differ in the NW Zagros, where the thickness and plasticity of the equivalent Infracambrian facies were probably insufficient to behave as a widespread tectonically active detachment layer (e.g. Kent 1970, 1979; Talbot & Alavi 1996).

Inherited extension and collisional inverted structures

For a long time, it has been envisioned that the present-day seismic activities of the Zagros reverse faults is due to inverse reactivation on pre-existing NE-dipping normal faults that were produced during the earlier Permian – Triassic rifting process (Jackson 1980; Jackson & McKenzie 1984). An integrated lithospheric modelling revealed a stretched continental crust with a thickness of *c.* 42 km beneath the Arabian Platform decreasing to *c.* 37 km beneath the Persian Gulf, as evidence for the Permian – Triassic rifting (Molinaro *et al.* 2005*b*), based on a combined interpretation of gravity, geoid, topography and isotherm curves. The recent studies on the structural styles and balancing cross-sections suggested that the belt has undergone two distinct episodes of crustal shortening across SE Zagros since the late Cenozoic collision (Molinaro *et al.* 2005*a*; Sherkati *et al.* 2005). First, during a Miocene – Pliocene thin-skinned phase, the main folded structures developed within the sedimentary cover. Second, during a Pliocene – Recent thick-skinned phase, the basement faults were reactivated as thrusts and created out-of-sequence structures, some of which cut obliquely through the earlier folded structures of the sedimentary cover. It is shown that the oblique out-of-sequence structures are characterized by major east – west reverse faults, which branch from the HZF in the HZB of SE Zagros in the Hadjiabad region (Fig. 18a; Molinaro *et al.* 2005*a*). This structural pattern can also be observed in the HZB of the Shahr-e-Kord region, to the NW of our study area (Fig. 18b). Ricou (1974) has already considered the east – west reverse faults of the HZB as reverse splays of the HZF, indicating transpressional deformation under the overall recent north – south compression associated with the right-lateral slip of the MRF (Authemayou *et al.* 2006). However, as mentioned elsewhere, the HZF is associated with a

Table 2. *Earthquake source parameters of the ZSFB of the Fars Arc*

Date	Time	Coordinates		*D*	M_w	Nodal plane 1			Nodal plane 2			*F*	P		N		T	
		Long. (E)	Lat. (N)			Strike	Dip	Rake	Strike	Dip	Rake		Dir.	Plunge	Dir.	Plunge	Dir.	Plunge
1977.10.19	06:35	55.12	27.57	15	5.5	117	41	120	259	56	66	R	006	08	273	19	117	69
1983.02.18	07:40	53.85	27.95	15	5.2	272	20	94	88	70	89	R	179	25	088	01	356	65
1984.12.22	16:05	53.68	27.51	49	5.1	115	41	84	303	49	95	R	029	04	120	04	255	85
1985.02.02	20:52	53.48	28.22	22	5.5	114	32	281	284	58	295	N	179	76	287	05	018	13
1985.08.07	15:43	52.89	27.72	15	5.6	303	39	116	91	55	70	R	195	08	103	16	311	72
1986.05.02	03:18	53.02	28.03	15	5.6	107	47	57	331	52	121	R	040	02	131	24	304	66
1986.05.03	10:37	53.00	27.90	15	5.2	111	33	60	325	62	108	R	042	15	136	16	270	68
1987.05.12	07:15	55.32	27.95	15	5.5	278	34	104	80	57	80	R	177	11	086	08	321	76
1990.11.06	18:45	55.25	28.06	15	6.6	274	37	107	73	55	77	R	172	09	080	10	302	76
1991.05.22	16:29	55.43	27.04	15	5.4	98	47	66	311	48	114	R	025	00	115	18	293	72
1992.05.19	12:24	55.35	28.05	15	5.6	254	40	99	63	51	83	R	158	05	067	06	291	82
1993.03.29	15:20	52.30	27.98	40	5.2	104	28	72	305	64	99	R	028	18	120	08	234	70
1993.07.09	10:29	55.51	28.45	23	5.2	110	26	120	257	68	76	R	357	22	262	13	144	65
1994.03.01	03:49	52.42	28.75	17	6.1	136	85	2176	46	86	25	S	001	06	190	84	091	01
1994.03.30	19:55	52.60	28.96	33	5.4	148	71	177	239	87	19	S	012	11	248	71	105	15
1995.01.24	04:14	55.65	27.64	15	5.0	217	31	56	75	64	109	R	151	17	247	17	018	65
1996.05.24	06:36	53.12	27.74	15	5.2	107	22	88	289	68	91	R	019	23	109	01	201	67
1997.05.05	15:11	53.42	27.16	15	5.1	296	52	128	64	52	52	R	180	00	090	29	270	61
1997.10.03	11:28	54.84	27.49	15	5.3	142	33	164	246	81	58	R	001	29	251	32	124	44
1998.11.13	13:01	53.38	27.52	33	5.4	103	35	78	298	56	98	R	022	11	113	07	235	77
1999.04.30	04:20	52.96	27.74	45	5.2	321	53	134	82	55	47	R	201	01	110	34	293	56
2000.03.01	20:06	52.85	28.40	15	5.0	49	26	55	267	69	106	R	345	23	081	14	201	63
2001.04.13	01:04	55.04	27.55	26	5.1	166	34	135	295	67	64	R	044	18	306	24	168	60
2003.07.10	17:06	54.10	28.35	15	5.8	277	33	93	93	57	88	R	185	12	094	02	355	78
2003.07.10	17:40	54.05	28.26	15	5.7	83	34	49	310	65	114	R	022	17	119	21	257	62
2003.10.24	05:58	53.91	28.34	33	5.0	128	39	70	333	54	105	R	052	08	144	12	290	75
2003.11.28	23:19	53.66	28.19	33	5.0	43	19	60	255	74	100	R	337	28	072	09	179	60
2003.12.15	22:57	53.86	28.39	15	5.1	272	43	90	92	47	90	R	182	02	092	00	001	88
2004.01.14	16:58	52.17	27.54	12	5.2	297	25	95	112	65	88	R	203	20	113	02	017	70
2005.08.09	05:09	52.52	28.90	16	5.1	257	30	31	139	75	117	R	209	25	312	26	081	53
2006.09.10	08:57	54.29	27.54	23	5.0	321	52	147	73	65	43	R	194	08	098	41	293	48

D, centroid depth (km). Nodal planes are shown by their strike and dip with the rake of slip vector. F, fault type (R, reverse; S, strike-slip; N, normal) P, N and T are pressure, neutral and tension axes, which are indicated by their direction and plunge. Source: Harvard CMT solution (http://www.seismology.harvard.edu). Site location is shown in Figure 16b.

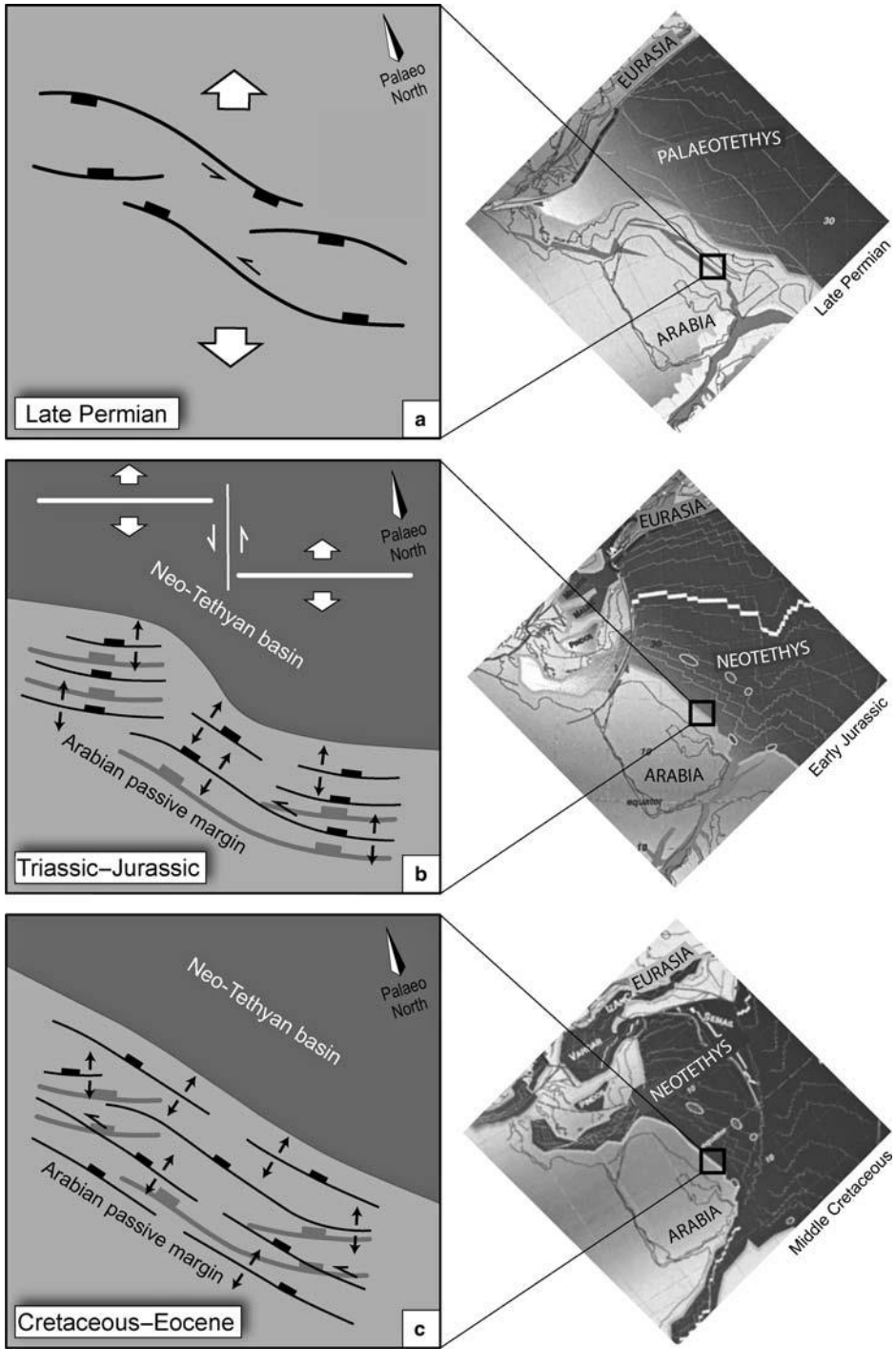

Fig. 17. Schematic illustration of a possible scenario for the Mesozoic extensional brittle tectonic evolution of the NEAPM. (a) Inferred Permian – Triassic oblique stretching that initiated major east – west normal faults within both the continental basement and the Palaeozoic sedimentary sequence close to the rift axis. (b) Continuation of margin-oblique faulting and extensional block tilting on the inherited normal faults, with some localized margin-parallel and

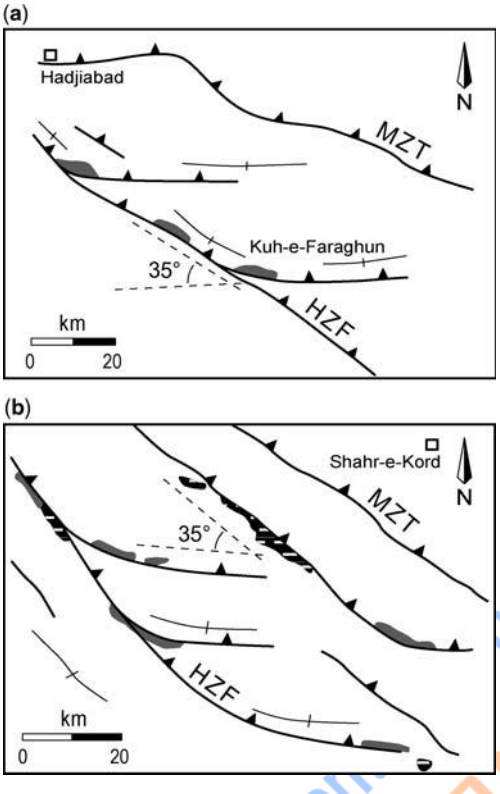

Fig. 18. Major reverse fault pattern of the HZB. (a) Out-of-sequence structures of the Hadjiabad area (after Molinaro *et al.* 2005*a*), indicating east – west reverse faults branching from the HZF at an acute angle of *c.* 35°, associated with the Permian – Triassic outcrops. Location is shown in Figure 1. (b) Structural map of the Shahr-e-Kord area (after NIOC 1975), indicating similar reverse fault pattern, associated with the Hormuz Salt plugs and Palaeozoic outcrops. Location is shown in Figure 15c. Description of outcrops as in Figure 2. Abbreviations as in Figure 1.

high degree of uplifting to the NE, separating the Mesozoic outcrops of the HZB from the Cenozoic ones of the ZSFB (see Fig. 2). The presence of outcrops of Palaeozoic sedimentary rocks, together with the existence of numerous Hormuz Salt plugs along both the HZF (e.g. Sepehr & Cosgrove 2004) and the corresponding east – west reverse faults throughout the HZB (Fig. 18a, b) imply involvement of the deep-seated basement structures in such a deformation.

We acknowledge that the east – west reverse faults of the HZB can be interpreted as reverse splays of the HZF as a result of a right-lateral transpressional deformation especially in the Shahr- e-Kord region. However, such a high right-lateral movement similar to the MRF was not observed in the field along the HZF, and the focal mechanisms determined for the earthquakes along the HZF invariably show basement reverse faulting (see Talebian & Jackson 2004) on pre-existing high-angle faults (Yamini-Fard *et al.* 2006). The angle between the trends of these two reverse fault sets is about 35°, similar to that already observed between both the Mesozoic normal faults of the HZB and the basement reverse faults of the ZSFB of Fars Arc (see Figs 9a, 15c, 16c & 18a, b). We could identify the inverse reactivation on some of the Mesozoic normal faults, as is characterized by the existence of both normal and reverse fault slip striations on the same fault planes at different sites (see Fig. 9c, d). Consequently, we prefer to interpret these reverse structures as the result of an inversion on the pre-existing deep-seated normal faults (i.e. the old half-graben structure of the NEAPM), as was suggested by Sepehr & Cosgrove (2004) based on interpretation of a seismic profile across one of the anticlines of the Dezful Embayment (see Fig. 12a). Numerical modelling of crustal stretching has already suggested that inversion structures depend strongly on the inherited extensional geometry during the subsequent contraction (Buiter *et al.* 2002). This evidence led us to infer that the present-day structural styles of the HZB, which developed during the late Cenozoic collision and the subsequent crustal shortening, are compatible with, and partly controlled by, the inherited Mesozoic structures. In other words, the pre-existing Mesozoic structures could have played an essential basic role in the late Cenozoic structural evolution, under differently oriented compressional stress trends (see Navabpour *et al.* 2006, 2007*a*).

Therefore, the Miocene – Pliocene thin-skinned shortening could have occurred by roll-back on the pre-existing NW – SE thin-skinned extensional brittle structures (i.e. the normal faults of the sedimentary cover; Fig. 19a) in the HZB, under a general NE – SW compressional stress trend during the first stages of continental collision. During this period, the MZT was the location of a southwestward active thrusting of the SSMZ over the HZB (Braud 1971; Agard *et al.* 2005). The inherited

Fig. 17. (*Continued*) oblique-slip faulting during the Triassic – Jurassic period. (c) Gradual change in the extensional tectonic regime, prevailing NW – SE margin-parallel faults with reactivation of the inherited margin-oblique faults inducing some oblique-slip normal movements during the Cretaceous – early Tertiary period. Light and dark grey backgrounds indicate continental and oceanic crust, respectively. Inherited faults and oceanic structures are marked as grey and white lines, respectively. Location maps from Stampfli & Borel (2002). Palaeo-north directions from Gaetani *et al.* (2003) after Dercourt *et al.* (2000). Arrows as in Figure 15.

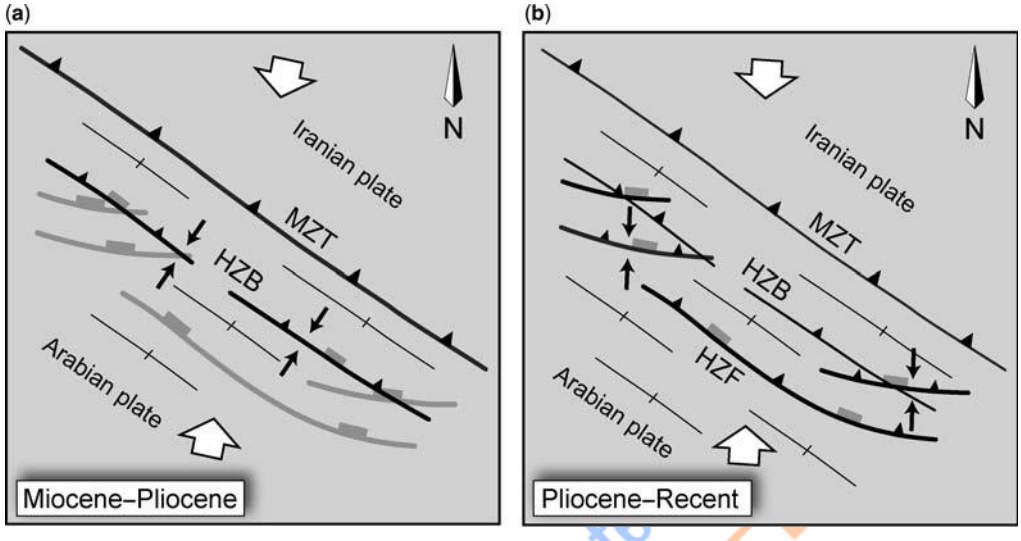

Fig. 19. Inversion of the inherited extensional structures during the late Cenozoic shortening of the Zagros in the HZB of interior Fars. (a) Thin-skinned inversion on the margin-parallel normal faults of the sedimentary cover. (b) Thick-skinned inversion on the margin-oblique normal faults of the basement. In each stage, bold black lines mark active reverse faults. Pairs of black arrows indicate direction of compression (from Navabpour *et al.* 2007*a*). Pairs of white arrows indicate direction of plate convergence (from McQuarrie *et al.* 2003). Other descriptions as in Figure 17. Location is shown in Figure 1; abbreviations as in Figure 1.

normal faults within the Mesozoic units could have facilitated deep ramps to develop and transfer the reverse displacement, detached from the basement by the basal Hormuz Salt horizon, to an upper flat detachment situated within the Upper Cretaceous Gurpi marls, producing the late Tertiary imbricate structure of the HZB (Molinaro *et al.* 2005*a*). The Pliocene – Recent thick-skinned shortening could have taken place by roll-back on the inherited east – west thick-skinned extensional brittle struc- tures (i.e. the normal faults of the basement; Fig. 19b), under the recent north – south compres- sional stress trend, creating the out-of-sequence high-angle reverse faults that cut obliquely through the earlier structures of the overlying sedimentary cover of the HZB. During this period, the activity of the MZT had ceased, as shown by the Upper Pliocene Bakhtyari deposits sealing the correspond- ing structures (Gidon *et al.* 1974*a*, *b*), and the HZF is known to have a significant present-day seismic reverse activity in the HZB (Yamini-Fard 2003; Yamini-Fard *et al.* 2006). Further south, in the ZSFB, the basement active reverse faulting is characterized by major topographic steps at the surface of the sedimentary cover (Mouthereau *et al.* 2007) and highlighted by the numerous present-day earthquakes, with focal mechanisms indicating an average N009**8** trend for the recent compressive stress axes across the Fars Arc (Zamani 2009).

Conclusion

According to our analysis of brittle structures and based on the field evidence of syndepositional normal faulting in the HZB of interior Fars, we can reconstruct an extensional tectonic model for the Mesozoic history of the NEAPM. The reconstruction of tectonic palaeostress regimes and the corresponding structural patterns revealed the existence of two major margin-oblique and margin-parallel Mesozoic normal fault systems within the sedimentary cover. Further evidence of the existence of a possible Neo-Tethyan oblique palaeo-oceanic spreading axis together with the structures of the basement suggest that the Mesozoic structural pattern of the NEAPM could have been originated by gravitational reactivation on similar structures within the basement, which were inherited from an oblique oceanic opening. In this model, it is assumed that an oblique stretching process initiated thick-skinned extensional brittle structures as deep-seated normal faults within both the continental basement and the Palaeozoic sedimentary cover during the Permian – Triassic period. The deformation then continued during the Mesozoic era, commonly inducing extensional block tilting along the major inherited normal faults above the basal Infra-cambrian salt detachment, characterizing a thin-skinned extension.

Despite the major differences in region, age and orientation, a striking similarity exists between the proposed extensional tectonic evolution during the Neo-Tethyan opening in the NEAPM and the present-day extension in the Aden Gulf of the south Arabian continental passive margin. In both cases, the continental break-up was oblique in type, involving both the normal and transform fault segments of the stretching basement. The initial direction of extension was thus close to that of the plate divergence, oblique to the forthcoming continental margins, initiating deep-seated margin-oblique normal faults within the continental basement. During the next steps of oceanic opening, the direction of extension became nearly perpendicular to the continental margin, as local extensional tectonic processes prevailed by margin-parallel normal faults within the sedimentary cover. We infer that such resemblances in structural evolution reflect a similar transition from margin-oblique to margin-perpendicular extension as an oblique oceanic opening continues.

Although more detailed brittle tectonic analysis is needed at the scale of the whole Zagros belt, our reconstruction also highlights the role of the inherited extensional brittle structures of both the basement and the sedimentary cover in the subsequent structural evolution characterized by the late Cenozoic collision and crustal shortening. Our fault slip data analysis strongly suggests that the inherited normal faults within the sedimentary sequence of the Arabian margin were reactivated as reverse faults during the folding process of the Miocene – Pliocene thin-skinned shortening. In the next stage of late Cenozoic compression, the out-of-sequence reverse structures related to the Pliocene – Recent thick-skinned shortening involved inversion of the inherited basement normal faults. The reactivated brittle structures were a function of both the inherited normal fault patterns and the late Cenozoic compressive stress orientations. Such a tectonic evolution, however, should not be extrapolated to other regions of the Zagros, where the basal salt detachment is absent or is of lesser importance.

We thank the Geological Survey of Iran (GSI) for providing vehicles and financial support during the extensive fieldwork in Iran. Trips to Iran were supported by the Middle East Basin Evolution (MEBE) project. Valuable comments by A. Zanchi and O. Bellier resulted in significant improvement of the manuscript, and M. Saadat proof-read the manuscript; their help is gratefully acknowledged. The senior author thanks the Cultural Service of the French Embassy in Tehran and the French Ministry of Foreign Affairs for thesis grant through the CNOUS – CROUS, enabling him to study in the University of Nice – Sophia Antipolis.

References

Agard, P., Omrani, J., Jolivet, L. & Mouthereau, F. 2005. Convergence history across Zagros (Iran): constraints from collisional and earlier deformation. ***International Journal of Earth Sciences***, 94, 401 – 419, doi: 10.1007/s00531-005-0481-4.

Agard, P., Monié, P. *et al.* 2006. Transient, synobduction exhumation of Zagros blueschists inferred from *P – T*, deformation, time, and kinematic constraints: Implications for Neotethyan wedge dynamics. ***Journal of Geophysical Research***, 111, B11401, doi: 10.1029/2005JB004103.

Angelier, J. 1984. Tectonic analyses of fault slip data sets. ***Journal of Geophysical Research***, 89, 5835 – 5848.

Angelier, J. 1990. Inversion of field data in fault tectonics to obtain the regional stress III. A new rapid direct inversion method by analytical means. ***Geophysical Journal International***, 103, 363 – 376.

Angelier, J. 2002. Inversion of earthquake focal mechanisms to obtain the seismotectonic stress IV. A new method free of choice among nodal planes. ***Geophysical Journal International***, 150, 588 – 609.

Angelier, J. & Bergerat, F. 1983. Systèmes de contrainte et extension intra-continentale. Colloque 'Rifts et Fossés Anciens', Marseille. ***Bulletins du Centre de Recherches Exploration–Production ELF-Aquitaine***, 7, 137 – 147.

Angelier, J. & Mechler, P. 1977. Sur une méthode graphique de recherche des contraintes principales également utilisable en tectonique et en séismologie: la méthode des dièdres droits. ***Bulletin de la Société Géologique de France***, 7, 1309 – 1318.

Angelier, J., Barrier, E. & Navabpour, P. 2006. Brittle tectonic analyses near Kermanshah and Shiraz – Neyriz, SW-Zagros, Iran: mesozoic extension across the Arabian margin. ***The Middle East Basin Evolution Conference Abstracts, December 2006, University of Milan, Milan***, 7 – 8.

Aubourg, C., Smith, B. *et al.* 2004. Post-Miocene shortening pictured by magnetic fabric across the Zagros – Makran syntaxis. ***In***: ***Orogenic Curvatures***. Geological Society of America, Special Papers, 383, 17 – 40.

Authemayou, C., Chardon, D., Bellier, O., Malekzadeh, Z., Shabanian, E. & Abbassi, M. R. 2006. Late Cenozoic partitioning of oblique plate convergence in the Zagros fold-and-thrust belt (Iran). ***Tectonics***, 25, TC3002, doi: 10.1029/2005TC001860.

Bakhtari, H., Frizon de Lamotte, D., Aubourg, C. & Hassanzadeh, J. 1998. Magnetic fabric of Tertiary sandstones from the Arc of Fars (Eastern Zagros, Iran). ***Tectonophysics***, 284, 299 – 316.

Béchennec, F., Le Métour, J., Rabu, D., Bourdillon-Jeudy-de-Grissac, C., De Wever, P., Beurrier, M. & Villey, M. 1990. The Hawasina Nappes: stratigraphy, palaeogeography and structural evolution of a fragment of the south-Tethyan passive continental margin. ***In***: Robertson, A. H. F., Searle, M. P. & Ries, A. C. (eds) ***The Geology and Tectonics of the Oman Region***. Geological Society, London, Special Publications, 49, 213 – 223.